Acknowledgements

We thank Dr A. Iwamatsu (Protein Research Network, Yokohama, Japan) for PMF analysis; Ms I. Temmoto (Hokkaido System Science, Sapporo, Japan) for microarray analysis; Mr Y. Yokoi, Ms. Y. Horiguchi, Mr R. Shirai, Ms. M. Ito and Dr Y. Fukui for technical assistance and discussion. This work was supported by the Meiyaku Open Research Project.

References

1 Kersten S, Desvergne B & Wahli W (2000) Roles of PPARs in health and disease. *Nature* **405**, 421–424.
2 Palmer CN, Hsu MH, Griffin KJ, Raucy JL & Johnson EF (1998) Peroxisome proliferator activated receptor-α expression in human liver. *Mol Pharmacol* **53**, 14–22.
3 Motojima K (2004) 17β-hydroxysteroid dehydrogenase type 11 is a major peroxisome proliferator-activated receptor α-regulated gene in mouse intestine. *Eur J Biochem* **271**, 4141–4146.
4 Mindnich R, Moller G & Adamski J (2004) The role of 17 β-hydroxysteroid dehydrogenases. *Mol Cell Endocrinol* **218**, 7–20.
5 Shafqat N, Marschall HU, Filling C, Nordling E, Wu XQ, Bjork L, Thyberg J, Martensson E, Salim S, Jornvall H & Oppermann U (2003) Expanded substrate screenings of human and Drosophila type 10 17β-hydroxysteroid dehydrogenases (HSDs) reveal multiple specificities in bile acid and steroid hormone metabolism: characterization of multifunctional 3α/7α/7β/17β/20β/21-HSD. *Biochem J* **376**, 49–60.
6 Chai Z, Brereton P, Suzuki T, Sasano H, Obeyesekere V, Escher G, Saffery R, Fuller P, Enriquez C & Krozowski Z (2003) 17 β-hydroxysteroid dehydrogenase type XI localizes to human steroidogenic cells. *Endocrinology* **144**, 2084–2091.
7 Lee SS, Pineau T, Drago J, Lee EJ, Owens JW, Kroetz DL, Fernandez-Salguero PM, Westphal H & Gonzalez FJ (1995) Targeted disruption of the α isoform of the peroxisome proliferator-activated receptor gene in mice results in abolishment of the pleiotropic effects of peroxisome proliferators. *Mol Cell Biol* **15**, 3012–3022.
8 Kersten S, Seydoux J, Peters JM, Gonzalez FJ, Desvergne B & Wahli W (1999) Peroxisome proliferator-activated receptor α mediates the adaptive response to fasting. *J Clin Invest* **103**, 1489–1498.
9 Zhang QY, Dunbar D & Kaminsky LS (2003) Characterization of mouse small intestinal cytochrome P450 expression. *Drug Metab Dispos* **31**, 1346–1351.
10 Bock KW (2003) Vertebrate UDP-glucuronosyltransferases: functional and evolutionary aspects. *Biochem Pharmacol* **66**, 691–696.
11 Volle DH, Repa JJ, Mazur A, Cummins CL, Val P, Henry-Berger J, Caira F, Veyssiere G, Mangelsdorf DJ & Lobaccaro JM (2004) Regulation of the aldo-keto reductase gene akr1b7 by the nuclear oxysterol receptor LXRα (liver X receptor-α) in the mouse intestine: putative role of LXRs in lipid detoxification processes. *Mol Endocrinol* **18**, 888–898.
12 Barbier O, Villeneuve L, Bocher V, Fontaine C, Torra IP, Duhem C, Kosykh V, Fruchart JC, Guillemette C & Staels B (2003) The UDP-glucuronosyltransferase 1A9 enzyme is a peroxisome proliferator-activated receptor α and γ target gene. *J Biol Chem* **278**, 13975–13983.
13 Demozay D, Rocchi S, Mas JC, Grillo S, Pirola L, Chavey C & Van Obberghen E (2004) Fatty aldehyde dehydrogenase: potential role in oxidative stress protection and regulation of its gene expression by insulin. *J Biol Chem* **279**, 6261–6270.
14 Tsuruoka N, Kidokoro A, Matsumoto I, Abe K & Kiso Y (2005) Modulating effect of sesamin, a functional lignan in sesame seeds, on the transcription levels of lipid- and alcohol-metabolizing enzymes in rat liver: a DNA microarray study. *Biosci Biotechnol Biochem* **69**, 179–188.
15 Kiso Y (2004) Antioxidative roles of sesamin, a functional lignan in sesame seed, and it's effect on lipid- and alcohol-metabolism in the liver: a DNA microarray study. *Biofactors* **21**, 191–196.
16 Hunt MC, Lindquist PJ, Peters JM, Gonzalez FJ, Diczfalusy U & Alexson SE (2000) Involvement of the peroxisome proliferator-activated receptor α in regulating long-chain acyl-CoA thioesterases. *J Lipid Res* **41**, 814–823.
17 Motojima K & Seto K (2003) Fibrates and statins rapidly and synergistically induce pyruvate dehydrogenase kinase 4 mRNA in the liver and muscles of mice. *Biol Pharm Bull* **26**, 954–958.
18 Shankar K, Vaidya VS, Corton JC, Bucci TJ, Liu J, Waalkes MP & Mehendale HM (2003) Activation of PPARα in streptozotocin-induced diabetes is essential for resistance against acetaminophen toxicity. *FASEB J* **17**, 1748–1750.
19 van Lieshout EM, Bedaf MM, Pieter M, Ekkel C, Nijhoff WA & Peters WH (1998) Effects of dietary anticarcinogens on rat gastrointestinal glutathione S-transferase θ 1–1 levels. *Carcinogenesis* **19**, 2055–2057.
20 Ohno S, Matsumoto N, Watanabe M & Nakajin S (2004) Flavonoid inhibition of overexpressed human 3β-hydroxysteroid dehydrogenase type II. *J Steroid Biochem Mol Biol* **88**, 175–182.
21 Shay NF & Banz WJ (2004) Regulation of gene transcription by botanicals: Novel regulatory mechanisms. *Annu Rev Nutr* **25**, 297–315.
22 Ferguson SS, LeCluyse EL, Negishi M & Goldstein JA (2002) Regulation of human CYP2C9 by the constitu-

tive androstane receptor: discovery of a new distal binding site. *Mol Pharmacol* **62**, 737–746.
23 Pascussi JM, Gerbal-Chaloin S, Drocourt L, Maurel P & Vilarem MJ (2003) The expression of CYP2B6, CYP2C9 and CYP3A4 genes: a tangle of networks of nuclear and steroid receptors. *Biochim Biophys Acta* **1619**, 243–253.
24 Jackson JP, Ferguson SS, Moore R, Negishi M & Goldstein JA (2004) The constitutive active/androstane receptor regulates phenytoin induction of Cyp2c29. *Mol Pharmacol* **65**, 1397–1404.
25 Anderson SP, Dunn C, Laughter A, Yoon L, Swanson C, Stulnig TM, Steffensen KR, Chandraratna RAS, Gustafsso JA & Corton JC (2004) Overlapping transcriptional programs regulated by the nuclear receptors peroxisome proliferator-activated receptor α, retinoid X receptor and liver X receptor in mouse liver. *Mol Pharm* **66**, 1440–1252.
26 Gerbal-Chaloin S, Pascussi JM, Pichard-Garcia L, Daujat M, Waechter F, Fabre JM, Carrere N & Maurel P (2001) Induction of CYP2C genes in human hepatocytes in primary culture. *Drug Metab Dispos* **29**, 242–251.
27 Nebert DW, Dalton TP, Okey AB & Gonzalez FJ (2004) Role of aryl hydrocarbon receptor-mediated induction of the CYP1 enzymes in environmental toxicity and cancer. *J Biol Chem* **279**, 23847–23850.
28 Bock KW & Kohle C (2004) Coordinate regulation of drug metabolism by xenobiotic nuclear receptors: UGTs acting together with CYPs and glucuronide transporters. *Drug Metab Rev* **36**, 595–615.
29 Xu C, Li CY & Kong AN (2005) Induction of phase I, II and III drug metabolism/transport by xenobiotics. *Arch Pharm Res* **28**, 249–268.
30 Barbier O, Fontaine C, Fruchart JC & Staels B (2004) Genomic and non–genomic interactions of PPARα with xenobiotic-metabolizing enzymes. *Trends Endocrinol Metab* **15**, 324–330.
31 Fuhr U (2000) Induction of drug metabolising enzymes: pharmacokinetic and toxicological consequences in humans. *Clin Pharmacokinet* **38**, 493–504.
32 Moore JT & Kliewer SA (2000) Use of the nuclear receptor PXR to predict drug interactions. *Toxicology* **153**, 1–10.
33 Motojima K (2000) Differential effects of PPARα activators on induction of ectopic expression of tissue-specific fatty acid binding protein genes in the mouse liver. *Int J Biochem Cell Biol* **32**, 1085–1092.
34 Motojima K, Passilly P, Peters JM, Gonzalez FJ & Latruffe N (1998) Expression of putative fatty acid transporter genes are regulated by peroxisome proliferator-activated receptor α and γ activators in a tissue- and inducer-specific manner. *J Biol Chem* **273**, 16710–16714.

Regulation of SR-BI protein levels by phosphorylation of its associated protein, PDZK1

Toshiyuki Nakamura*, Norihito Shibata*†, Takako Nishimoto-Shibata*, Dongdong Feng*, Mamoru Ikemoto*, Kiyoto Motojima‡, Naoyuki Iso-o§, Kazuhisa Tsukamoto§, Masafumi Tsujimoto†, and Hiroyuki Arai*¶

*Department of Health Chemistry, Graduate School of Pharmaceutical Sciences, University of Tokyo, Bunkyo-ku, Tokyo 113-0033, Japan; †Laboratory of Cellular Biochemistry, RIKEN, Wako-shi, Saitama 351-0198, Japan; ‡Department of Biochemistry, Meiji Pharmaceutical University, Kiyose-shi, Tokyo 204-8588, Japan; and §Department of Metabolic Diseases, Graduate School of Medicine, University of Tokyo, Bunkyo-ku, Tokyo 113-8655, Japan

Communicated by John A. Glomset, University of Washington, Seattle, WA, August 5, 2005 (received for review April 12, 2005)

Scavenger receptor class B type I (SR-BI) is a high-density lipoprotein (HDL) receptor that mediates the selective uptake of HDL cholesterol and cholesterol secretion into bile in the liver. Previously, we identified an SR-BI-associated protein, termed PDZK1, from rat liver membrane extracts. PDZK1 contains four PSD-95/Dlg/ZO-1 (PDZ) domains, the first of which in the N-terminal region is responsible for the association with SR-BI. PDZK1 controls hepatic SR-BI expression in a posttranscriptional fashion both in cell culture and *in vivo*. In this study, we demonstrated that the C-terminal region of PDZK1 is crucial for up-regulating SR-BI protein expression. Metabolic labeling experiments and phosphoamino acid analysis revealed that PDZK1 is phosphorylated at Ser residues within this region. Point-mutation analysis demonstrated that PDZK1 is phosphorylated at Ser-509. Interestingly, a mutant PDZK1, in which Ser-509 was replaced with Ala, lost the ability to up-regulate SR-BI protein. We identified Ser-509 of PDZK1 as the residue that is phosphorylated by the cAMP-dependent PKA *in vitro* as well as in cell culture. Ser-509 of PDZK1 in rat liver was also phosphorylated, as shown by an Ab that specifically detects phosphorylated Ser-509. Administration of glucagon to Wistar rats increased PDZK1 phosphorylation as well as hepatic SR-BI and PDZK1 expression while it decreased plasma HDL levels, indicating that PDZK1 phosphorylation is hormonally regulated. These findings suggest that phosphorylation of PDZK1 has an important role in the regulation of hepatic SR-BI expression and, thus, influences plasma HDL levels.

glucagon | high-density lipoprotein | PKA

Plasma high-density lipoprotein (HDL) has a critical role in cholesterol metabolism, and plasma HDL concentrations are inversely related to the risk of developing cardiovascular disease (1, 2). The protective role of HDL against cardiovascular disease is commonly attributed to its ability to remove excess cholesterol from cells in the arterial wall and transport it to the liver for disposal, which is a process that is called reverse cholesterol transport (3, 4). Scavenger receptor class B type I (SR-BI) is an HDL receptor that is expressed in the liver as well as in steroidogenic tissues at high levels and mediates the selective uptake of HDL cholesterol (5, 6). Overexpression of SR-BI in murine hepatocytes results in the virtual disappearance of plasma HDL and a substantial increase in biliary cholesterol (7–10). Mice with a targeted mutation in the *SR-BI* gene exhibit increased plasma HDL cholesterol levels, increased HDL particle size (11, 12), and impaired biliary cholesterol secretion (13). These studies have established the concept that SR-BI determines the level of plasma HDL by taking up HDL cholesterol into the liver for transport into bile.

SR-BI contains a large extracellular domain that is anchored in the plasma membrane by transmembrane domains adjacent to short cytoplasmic N- and C-terminal regions (6). We have identified (14) an SR-BI C-terminal binding protein from rat liver membranes and named it CLAMP (C-terminal linking and modulating protein). CLAMP contains four PSD-95/Dlg/ZO-1 (PDZ) domains and associates with the C terminus of SR-BI via its N-terminal first PDZ domain (14). CLAMP is expressed mainly in the liver, kidney, and small intestine, whereas steroidogenic organs that express high levels of SR-BI, such as the adrenal grand, showed no significant CLAMP expression (15, 16). This protein has been shown to interact with a number of membrane-associated transporter proteins from different tissues, such as cMOAT/MRP2 (17), cystic fibrosis transmembrane regulator (CFTR) (16), CIC-3B (18), type IIa Na^+/P_i cotransporter (Na/P_i-IIa) (19), solute carrier SLC17A1 (Na/P_i-I), Na^+/H^+ exchanger (NHE-3), organic cation transporter (OCTN), chloride–formate exchanger (CFEX), and urate–anion exchanger (URAT1) (20). CLAMP is also called diphor-1 (21), PDZK1 (15), CAP70 (16), and NaPi-Cap1 (19), depending on its binding partners. Here, we refer to CLAMP as PDZK1.

In recent studies, Kocher *et al.* showed that PDZK1 knockout mice had significantly increased plasma cholesterol levels (22) as well as dramatically reduced hepatic SR-BI protein levels and abnormally large HDL particles in plasma (23). Similar changes were observed in SR-BI knockout mice (11). These studies established that PDZK1 up-regulates hepatic SR-BI expression at the protein level *in vivo*. Consistent with these observations, we have demonstrated (14) that coexpression of PDZK1 and SR-BI in CHO cells results in increased SR-BI protein levels without affecting the SR-BI mRNA level.

In this study, we searched for other domains, in addition to the N-terminal first PDZ domain in PDZK1, that are required for its SR-BI up-regulating activity. We found evidence that phosphorylation of the PDZK1 C-terminal region is also involved in the up-regulation of SR-BI protein expression.

Materials and Methods

Cells. CHO-K1 cells were grown in Ham's F-12 medium, supplemented with 10% FCS, 50 units/ml penicillin, 50 mg/ml streptomycin, and 2 mM glutamine at 37°C in a humidified 5% CO_2/95% air incubator. Rat hepatoma Fao cells were maintained in Coon's F-12 medium supplemented with 10% FCS, 50 units/ml penicillin, 50 mg/ml streptomycin, and 2 mM glutamine at 37°C in a humidified 10% CO_2/90% air incubator.

Creation of PDZK1 Mutants. PDZK1 mutations were constructed by PCR-mediated mutagenesis. All cDNAs were cloned into pcDNA 3.1/Hygro (Invitrogen), pGEX6P-1 (Amersham Biosciences), or pShuttle-CMV (Q-BIO Gene, Carlsbad, CA) and verified by sequencing. Fusion proteins of GST were expressed in *Escherichia coli* and purified as described (14). The shuttle

Abbreviations: HDL, high-density lipoprotein; PDZ, PSD-95/Dlg/ZO-1; CLAMP, C-terminal linking and modulating protein; pAb, polyclonal Ab; CBB, Coomassie brilliant blue; SR-BI, scavenger receptor class B type I.

¶To whom correspondence should be addressed. E-mail: harai@mol.f.u-tokyo.ac.jp.

www.pnas.org/cgi/doi/10.1073/pnas.0506679102

vector plasmids were inserted into pAdEasy-1 (Q-BIO Gene). Recombinant adenoviral constructs were transfected into E1-transformed human embryonic kidney (HEK293ΔE1) cells to produce viral particles. The recombinant adenoviruses were purified by cesium chloride ultracentrifugation. As controls, the LacZ virus that carries β-gal cDNA was also constructed and purified as described above.

Transfection of Plasmids and Transduction of Adenoviral Vectors into Cells. CHO-K1 cells were transfected with Lipofectamine 2000 (Invitrogen) according to the manufacturer's protocol. Constitutively transfected cells were selected with hygromycin. Cultured Fao cells at 70% confluence were infected with the respective adenoviruses at a rate of 5,000 particles per cell in Coon's F-12 medium containing 2% FBS for 2 h. The cultures were supplemented an equal volume of Coon's F-12 medium containing 20% FBS and incubated for an additional 4 days.

Preparation of Rat Liver Membrane Extracts. Livers obtained from male Wistar rats (200–250 g, 8 weeks old) were homogenized with a homogenizing buffer (14), and the homogenate was centrifuged at 100,000 × *g* for 1 h at 4°C. The resulting precipitate was suspended in a homogenizing buffer.

Ab Production. A synthetic phosphopeptide based on residues 503–514 of rat PDZK1 with phospho-Ser-509 was conjugated to keyhole limpet hemocyanin [KLH-CARDRTLS (PO_3H_2) AASHS] and injected subcutaneously into rabbits together with adjuvants. After eight booster injections at weekly intervals, anti-509-P-PDZK1 polyclonal Ab (pAb) was purified from rabbit serum by using a peptide-ligand-affinity column.

Western Blot Analysis. Proteins in the cell lysates or rat liver membrane extracts were separated by SDS/PAGE. The gels were blotted to polyvinylidene difluoride membranes (Millipore). The membranes were treated with anti-SR-BI pAb (NB400-101, Novus Biologicals, Littleton, CO), anti-PDZK1 mAb (14), or anti-509-P-PDZK1. The immunoreactive proteins were visualized by using chemiluminescence and recorded with a digital recorder (LAS-1000, Fuji Film, Tokyo). The relative amounts of proteins were quantified by using IMAGE GAUGE V.3.45 (Fuji Film).

Metabolic Labeling, Immunoprecipitation, and Phosphoamino Acid Analysis. CHO-K1 cells expressing PDZK1 or mutants of PDZK1 were incubated for 30 min in phosphate-depleted DMEM. Cultures were then labeled in labeling media containing 0.3 mCi (1 Ci = 37 GBq) of [^{32}P]orthophosphate for 4 h. Cells were lysed in immunoprecipitation buffer (0.5% Nonidet P-40/1% Triton X-100/10 mM Tris·HCl, pH 7.4/1 mM EDTA/150 mM NaCl/0.2 mM sodium vanadate/10 mM NaF/1 μg/ml pepstatin/1 μg/ml leupeptin/2 μg/ml aprotinin/1 mM PMSF). Lysates were immunoprecipitated with anti-PDZK1 mAb, as described in ref. 14. The immunoprecipitates were then analyzed by Western blotting and autoradiography. Phosphoamino acid maps of phosphorylated PDZK1 were generated by excising ^{32}P-labeled PDZK1 bands from polyvinylidene difluoride membranes and eluting the proteins with 6 M HCl for 1 h at 100°C. The samples were dried in a SpeedVac concentrator (Savant) and dissolved in first-dimension buffer [2.2% (vol/vol) formic acid/7.8% (vol/vol) acetic acid, pH 1.9], each sample containing three phosphoamino-acid standards (phospho-Ser, phospho-Thr, and phospho-Tyr). Phosphoamino acids were subjected to two-dimensional electrophoresis on TLC cellulose plates (pH 1.9, 1.5 kV for 30 min; pH 3.5, 1.3 kV for 15 min), followed by ninhydrin staining. The TLC plates were scanned with a BAS 2000 imaging system (Fuji Film) to detect labeled phosphoamino acids.

***In Vitro* Phosphorylation of PDZK1 by PKA.** We incubated 1 μg of recombinant GST-fused wild-type PDZK1 protein or GST-fused mutant PDZK1 protein, in which Ser-509 was replaced with Ala (S509A), with 5 units of cAMP-dependent PKA (Sigma) in phosphorylation buffer (50 mM Tris·HCl, pH 7.5/2 mM EDTA/7 mM $MgCl_2$/0.1 mM DTT/1 mM PMSF). We then added [γ-^{32}P]ATP (6 μCi), and the mixture was incubated at 30°C for 30 min. The reaction was stopped by boiling for 5 min in SDS sample buffer. The samples were subjected to SDS/PAGE and then stained with Coomassie brilliant blue (CBB). The gels were scanned with BAS 2000 to detect labeled PDZK1.

Phosphorylation of PDZK1 by PKA in Cell Culture. CHO-K1 cells stably expressing PDZK1 were treated with 10 μM forskolin (a PKA inducer) or 10 μM H-89 (a PKA inhibitor) and then labeled in labeling media containing 0.3 mCi of [^{32}P]orthophosphate for 4 h. Cells were lysed and immunoprecipitated with PDZK1. The immunoprecipitates were separated by SDS/PAGE. The gel was stained with CBB and scanned with BAS 2000 to detect labeled PDZK1.

Glucagon Administration. Male Wistar rats (200–250 g, 8 weeks old) were used. Animals were kept under standardized conditions with free access to water and chow. The light-cycle was from 7 a.m. to 7 p.m. Rats were injected s.c. under light ether anesthesia at 10 a.m. and 4 p.m. with 400 μg (115 nmol) of glucagon or a vehicle on each of 2 consecutive days. The blood was removed by venipuncture of the orbital sinus at 12 a.m., which was 2 h after the last injection. Then, rats were immediately killed, and livers were removed. Plasma was separated by low-speed centrifugation for 10 min at 4°C. Plasma total cholesterol and HDL cholesterol were prepared and assayed by using the cholesterol test kit (Wako Pure Chemical, Osaka).

Quantitative RT-PCR. Total RNA of rat liver was isolated with Isogen reagent (Nippon Gene, Toyama, Japan). Total RNA (1 μg) was reverse-transcribed in the presence of poly(dT) sequences in a total volume of 10 μl. We used 1 μl of this mixture as template in the quantitative RT-PCR. Quantitative RT-PCR reactions were performed by using the Prism 7000 sequence-detection system (Applied Biosystems). The following PCR primers were used: β-actin, 5-CCTTCTACAATGAGCTGCGTGT-3 (forward) and 5-TGGGGTGTTGAAGGTCTCAAAC-3 (reverse); SR-BI, 5-TTCTGGTGCCCATCATTTACC-3 (forward) and 5-AGCCCTTTTTACTACCACTCCAAA-3 (reverse); and CLAMP, 5-TTGAAGTGAATGGAGAAAATGTAG-3 (forward) and 5-TGATACGGCTTCCTGACTTTGTC-3 (reverse). Results were normalized to β-actin data.

Results

The PDZK1 C-Terminal Domain Is Required for Up-Regulation of SR-BI Expression. CHO-K1 cells expressing various deletion mutants of PDZK1 were established (Fig. 1*A*) and transiently transfected with SR-BI. SR-BI protein expression increased 4- to 5-fold in the cells coexpressing SR-BI and full-length PDZK1 (Fig. 1*B*). We also examined the effect of PDZK1 on SR-BI expression using rat hepatoma Fao cells, which intrinsically express SR-BI but not PDZK1. Expression of PDZK1 in Fao cells was achieved by infection with an adenovirus vector. The same degree of up-regulation of SR-BI protein was observed in this hepatoma cell line (Fig. 1*C*). However, none of the PDZK1 deletion mutants lacking the C-terminal region were able to up-regulate the SR-BI protein (Fig. 1*B*). Even the mutant lacking only 66 aa at the C terminus was less effective than the full-length PDZK1. These results suggest that PDZK1 is capable of up-regulating the SR-BI protein and that a region within the C-terminal 66 aa is indispensable for the up-regulation.

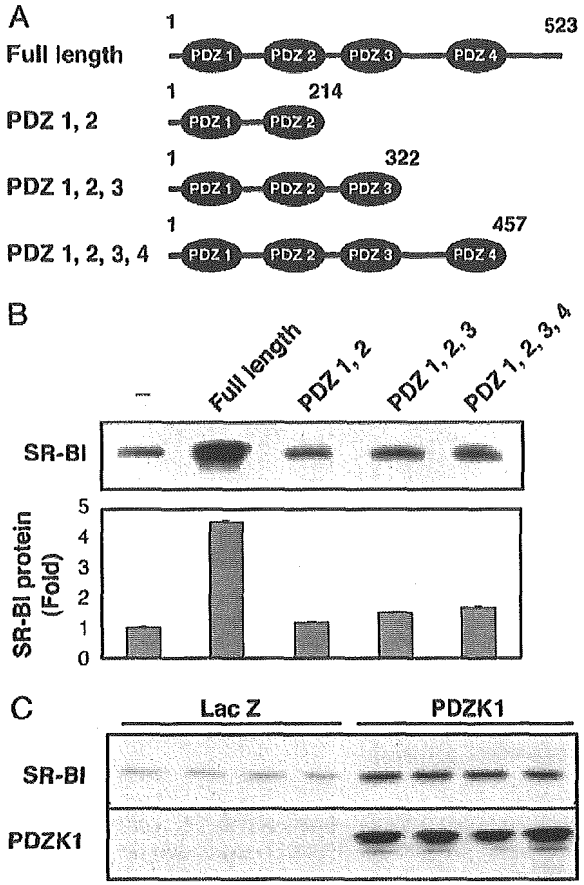

Fig. 1. The C-terminal region of PDZK1 is required for SR-BI up-regulation. (*A*) Schematic representation of various deletion mutants of PDZK1. (*B*) Western blot analysis of SR-BI from CHO-K1 cells constitutively expressing various deletion mutants of PDZK1 and transiently transfected with SR-BI. The graph represents relative quantities of SR-BI proteins in these Western blot analyses. (*C*) Western blot analysis of SR-BI and PDZK1 from cell lysates of Fao cells transduced with the recombinant adenovirus construct of PDZK1. LacZ is a control. The data represent at least three independent experiments.

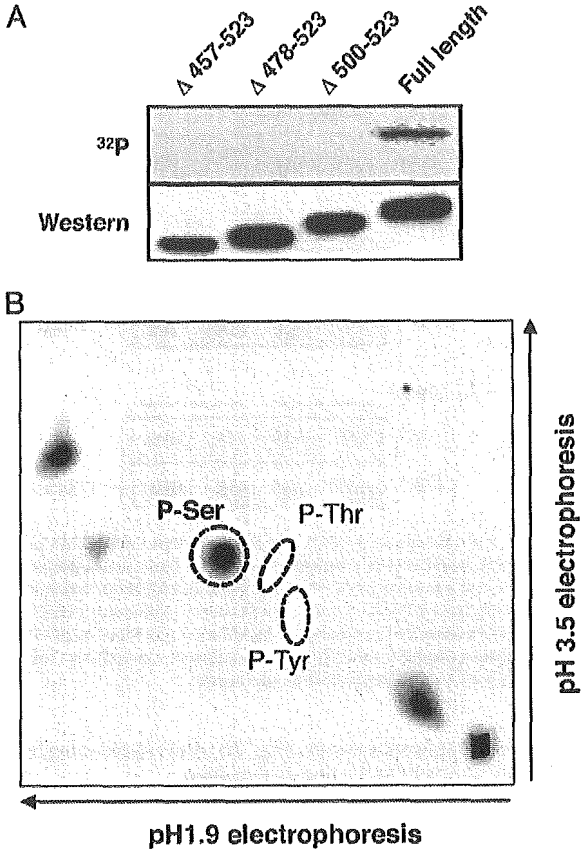

Fig. 2. PDZK1 is a phosphorylated protein. (*A*) Autoradiography (*Upper*) and the Western blot analysis of PDZK1 (*Lower*). CHO-KI cells were transiently transfected with an expression plasmid of C-terminal deletion mutants of PDZK1 (Δ457–523, Δ478–523, and Δ500–523) and incubated with [^{32}P]orthophosphate. (*B*) Phosphoamino acid analysis of ^{32}P-labeled PDZK1. Circles indicate where the phosphoamino acid standards migrated. P-Ser, phospho-Ser; P-Thr, phospho-Thr; P-Tyr, phospho-Tyr.

PDZK1 Is Phosphorylated at the Ser Residue in the C-Terminal Region. PDZK1 possesses multiple potential phosphorylation sites within the C-terminal 66 aa, as indicated by the NetPhos database (available at www.cbs.dtu.dk/services/NetPhos). To examine whether the C-terminal region of PDZK1 is phosphorylated in cells, we constructed three C-terminal deletion mutants (namely, Δ457–523, Δ478–523, and Δ500–523), corresponding to deletions of the indicated amino acids. The C-terminal deletion mutants and full-length PDZK1 were transfected into CHO-KI cells and metabolically labeled with [^{32}P]orthophosphate. The expressed proteins were immunoprecipitated with anti-PDZK1 mAb. Western blotting with the anti-PDZK1 mAb revealed that similar levels of wild-type and mutant PDZK1 proteins were expressed (Fig. 2*A*). A ^{32}P-labeled protein band comigrating with PDZK1 was detected in the CHO cell extract, indicating that PDZK1 is a phosphorylated protein. However, all of the tested C-terminal deletion mutants resulted in significant reduction of ^{32}P-labeling. These data demonstrate that the phosphorylation of PDZK1 occurs in a region within the C-terminal 66 aa.

We then analyzed phosphoamino acids of PDZK1 labeled with [^{32}P]orthophosphate. As shown in Fig. 2*B*, PDZK1 was phosphorylated on Ser residues but not on Thr or Tyr residues.

Ser-509 of PDZK1 Is Phosphorylated. Based on the database search for potential phosphorylation sites within the C-terminal 66 aa, we chose three potential sites of Ser phosphorylation (namely, Ser-509, Ser-516, and Ser-518). To determine whether these Ser residues were phosphorylated, we constructed respective Ala substitution mutants as shown in Fig. 3*A*. Transfection with these mutants into CHO-KI cells and metabolic labeling with ^{32}P revealed that S509A was no longer phosphorylated in transfected cells, whereas S516A

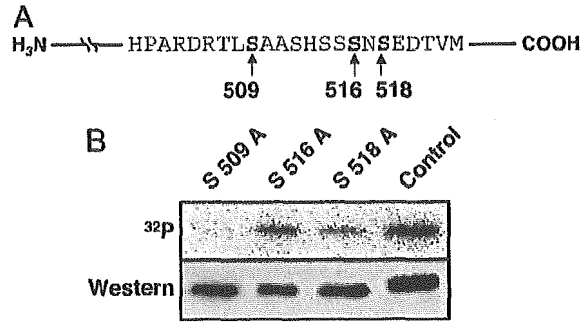

Fig. 3. Ser-509 of PDZK1 is phosphorylated. (*A*) Schematic representation of potential sites of Ser phosphorylation in the PDZK1 C-terminal region. (*B*) Autoradiography (*Upper*) and the Western blot analysis of PDZK1 (*Lower*). CHO-KI cells were transiently transfected with various single-point mutants of PDZK1 (S509A, S516A, and S518A) and labeled with [^{32}P]orthophosphate.

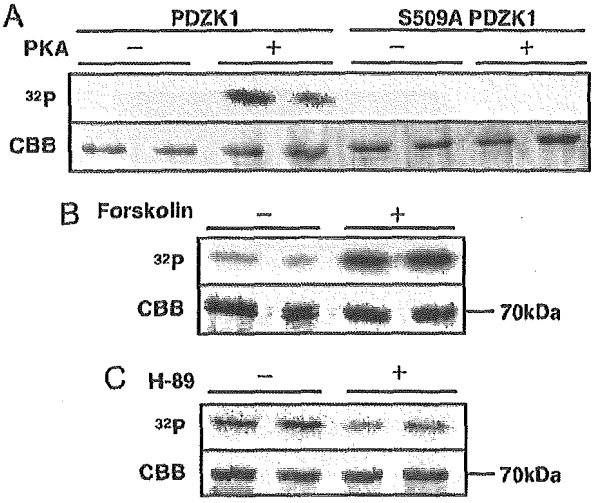

Fig. 4. PKA phosphorylates PDZK1. (*A*) Recombinant GST-PDZK1 or GST-S509A mutant fused protein expressed by *E. coli* was incubated with or without PKA in the presence of [γ-^{32}P]ATP. (*B* and *C*) Metabolic labeling with [^{32}P]orthophosphate of CHO-K1 cells constitutively expressing PDZK1 were performed in the absence or presence of 10 μM forskolin (*B*) or 10 μM H-89 (*C*). Autoradiography (*Upper*) and CBB staining (*Lower*) are shown. The data represent at least three independent experiments.

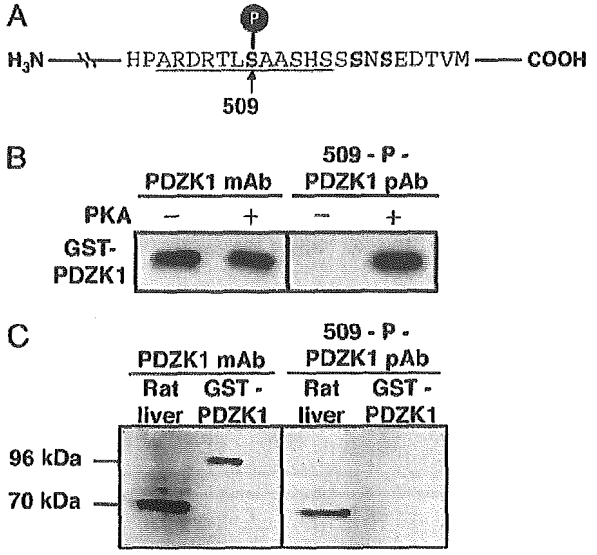

Fig. 5. PDZK1 expressed in the liver is phosphorylated *per se*. (*A*) Preparation of Abs against phospho-Ser-509. The underlined phosphorylated peptide was synthesized for immunization. (*B*) The recombinant PDZK1 expressed by *E. coli* was incubated with or without PKA and then subjected to Western blotting using anti-PDZK1 mAb (*Left*), anti-509-P-PDZK1 pAb (*Right*). (*C*) Western blot analysis of PDZK1 from rat liver membrane extract (70 kDa) and the recombinant GST-PDZK1 fused protein (96 kDa) using anti-PDZK1 mAb (*Left*) and anti-509-P-PDZK1 pAb (*Right*).

and S518A were phosphorylated (Fig. 3*B*), thus implicating Ser-509 as a critical site of PDZK1 phosphorylation.

PDZK1 Ser-509 Is Phosphorylated by PKA *in Vitro* and in Cell Culture. According to ref. 24, Ser-509 was found to be a potential PKA target Ser. To examine whether Ser-509 can be directly phosphorylated by PKA, we incubated the recombinant PDZK1 with the purified catalytic subunit of PKA in the presence of [γ-^{32}P]ATP. We found that PKA phosphorylated PDZK1 *in vitro*, whereas PKA did not phosphorylate the S509A mutant to any extent (Fig. 4*A*). Next, we treated CHO-K1 cells that constitutively express PDZK1 with the PKA inducer forskolin or the PKA inhibitor H-89 in the presence of [^{32}P]orthophosphate. Endogenous PDZK1 was then immunoprecipitated and subjected to CBB staining and autoradiography. The CBB-stained ≈70-kDa band was found to be PDZK1, as judged from the fact that this ≈70-kDa band in SDS/PAGE (Fig. 4 *B* and *C Lower*) reacted with anti-PDZK1 Ab by Western blot analysis and could not be detected by performing the same procedures with parental CHO-K1 cells (data not shown). Phosphorylation levels of PDZK1 were significantly increased by forskolin (Fig. 4*B*) and reduced by H-89 (Fig. 4*C*). These *in vitro* and cell-culture experiments demonstrated that PDZK1 Ser-509 is phosphorylated by PKA.

PDZK1 Expressed in Liver Is Phosphorylated. Although mutagenesis studies using CHO-K1 cells showed the importance of the Ser site for PDZK1 phosphorylation, it was not clear whether Ser-509 was phosphorylated *in vivo*. To answer this question, we established specific Abs against synthetic peptides corresponding to amino acids 503–514 of rat PDZK1 in which Ser-509 was phosphorylated (Fig. 5*A*). By using a phospho-specific Ab (anti-509-P-PDZK1) that was developed to detect Ser-509 phosphorylation, a prominent immunoreactive band was detected in the recombinant PDZK1 when the recombinant PDZK1 was incubated with PKA, whereas no anti-509-P-PDZK1 immunoreactivity was detected when the recombinant PDZK1 was incubated without PKA (Fig. 5*B*). In a Western blot analysis (Fig. 5*C*), anti-509-P-PDZK1 detected PDZK1 in rat liver extract but not the recombinant PDZK1 produced by *E. coli*. These results showed that Ser-509 of PDZK1 expressed in rat liver was phosphorylated.

SR-BI Protein Level Is Affected by the PDZK1 Phosphorylation State. Because we found that PDZK1 is phosphorylated at position Ser-509, we examined next whether PDZK1 phosphorylation could regulate SR-BI protein expression. Wild-type PDZK1 and the PDZK1 S509A mutant were overexpressed in rat hepatoma Fao cells by using recombinant adenovirus vectors (Fig. 6). The amount of SR-BI protein increased ≈4-fold in Fao cells transduced with an adenovirus vector harboring PDZK1 (Ad-PDZK1), as compared with Ad-LacZ. However, transduction of Fao cells with Ad-PDZK1 S509A mutant did not affect the amount of SR-BI protein. These results suggested that PDZK1 phosphorylation of Ser-509 is one of the key factors regulating SR-BI protein levels.

Glucagon Increases PDZK1 Phosphorylation as Well as Hepatic SR-BI Expression. Next, we investigated physiological conditions regulating PDZK1 phosphorylation in rat liver. Reports (25–28) have indicated that the administration of glucagon to laboratory

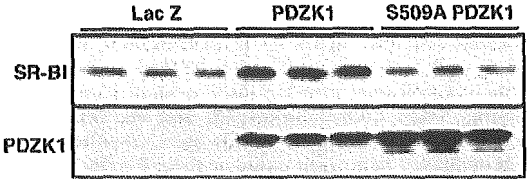

Fig. 6. SR-BI protein level is regulated by PDZK1 through phosphorylation. Western blot analysis of SR-BI (*Upper*) and PDZK1 (*Lower*) from cell lysates of Fao cells transduced with the recombinant adenovirus of PDZK1 or S509A PDZK1. LacZ is a control. The results of this figure are representative of at least three independent experiments.

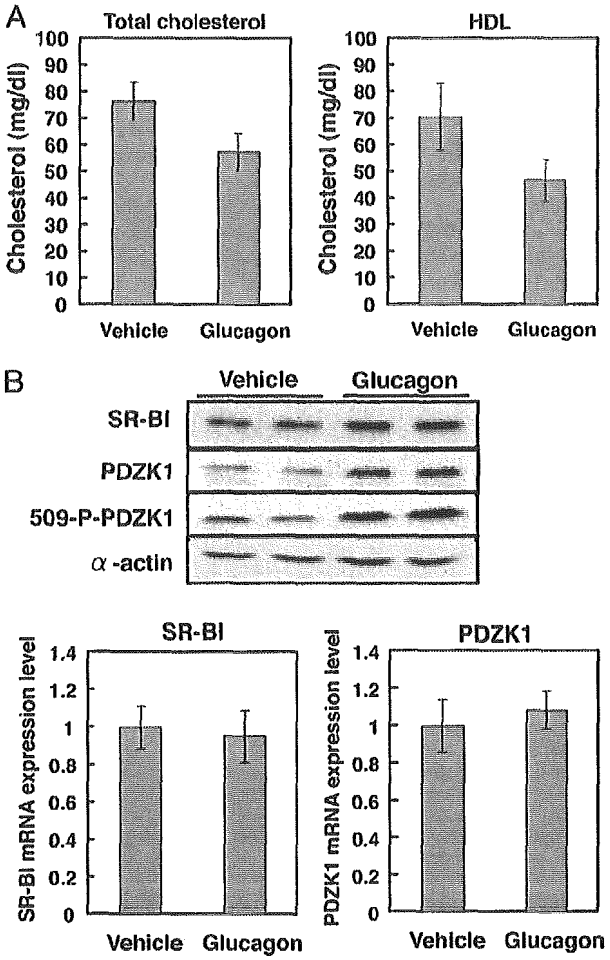

Fig. 7. Glucagon increases PDZK1 phosphorylation and hepatic SR-BI expression. Five rats were injected twice daily with 400 μg of glucagon or a vehicle for 2 days. Rats were killed 2 h after the last injection. (*A*) Total and HDL cholesterol levels. (*B*) Western blot analysis of SR-BI, PDZK1, phosphorylated PDZK1, and α-actin from rat liver homogenates of two representative animals. (*C*) Quantitative analysis of SR-BI and PDZK1 transcripts. Total RNA purified from rat liver was subjected to real time RT-PCR for measuring SR-BI and PDZK1 transcripts, as described in *Materials and Methods*.

animals as well as humans decreases plasma HDL cholesterol levels. To our knowledge, no information is available regarding the effects of glucagon on hepatic SR-BI *in vivo*. The actions of glucagon are mediated by the glucagon receptor linked to a heterotrimeric G-protein complex, leading to increased cellular levels of cAMP and activation of PKA. We hypothesized that the reduction of plasma levels of HDL by glucagon is due to the up-regulation of SR-BI protein expression through PDZK1 phosphorylation by PKA.

To determine the influence of glucagon on hepatic SR-BI expression and PDZK1 phosphorylation, rats were injected twice daily with 400 μg of glucagon or a vehicle for 2 days before they were killed. Total plasma cholesterol levels and plasma HDL cholesterol levels were decreased significantly, as reported in ref. 28 (Fig. 7*A*). Upon glucagon treatment, the phosphorylated form of PDZK1 was increased by 3.6 ± 0.2, whereas SR-BI and PDZK1 protein levels were increased by 1.8 ± 0.3 and 1.8 ± 0.4, respectively. Glucagon treatment did not affect SR-BI and PDZK1 mRNA levels (Fig. 7*C*), indicating the posttranscriptional regulation of hepatic SR-BI and PDZK1 expression by this hormone. These results suggested that PDZK1 phosphorylation and protein expression were hormonally regulated, and that up-regulation of hepatic SR-BI expression by glucagon is at least partly due to elevation of PDZK1 phosphorylation and/or its protein expression.

Discussion

We previously showed that coexpression of PDZK1 and SR-BI in CHO cells resulted in up-regulation of SR-BI protein expression without affecting the SR-BI mRNA level (14). Moreover, Kocher *et al.* (23) demonstrated that there is a 95% reduction in SR-BI protein expression in the livers of PDZK1-deficient mice compared with wild-type controls. These *in vitro* and *in vivo* data indicate that PDZK1 controls hepatic expression of SR-BI in a posttranscriptional fashion. In this study, we demonstrated that the phosphorylation of Ser-509 in the C-terminal region of PDZK1 is required for SR-BI up-regulation in cultured hepatoma cells. By using a phospho-specific Ab developed to detect Ser-509 phosphorylation, we showed that Ser-509 of hepatic PDZK1 is phosphorylated.

Three lines of evidence suggest that Ser-509 of PDZK1 is phosphorylated by PKA. First, the sequence around Ser-509 matches the potential phosphorylation site of PKA. Second, the recombinant PDZK1 is phosphorylated by PKA *in vitro*. Third, the phosphorylation level of PDZK1 in cultured cells is increased by a PKA activator and reduced by a PKA inhibitor. It has been demonstrated that the dual-specific A kinase-anchoring protein 2 (D-AKAP2), a member of the PKA-anchoring protein family (AKAP) binds to the fourth PDZ domain of PDZK1 in the kidney (20, 29), which is close to the Ser-509 position. D-AKAP2 is also expressed in the liver (30). It remains to be determined whether it interacts with PDZK1 in the liver.

The sequence around Ser-509 of PDZK1 also matches the consensus phosphorylation motif for p70 S6 kinase (p70S6K) (24). Interestingly, the C-terminal region of p70S6K contains a sequence capable of binding to a PDZ domain. Indeed, p70S6K has been reported (31) to interact with a PDZ domain-containing protein, called Neurabin, that exists in neuronal cells. In preliminary experiments, we found that p70S6K can phosphorylate Ser-509 in PDZK1 *in vitro*. Stimulation of hepatoma cells with insulin is known to activate p70S6K (32). Therefore, it is plausible that diverse extracellular events can lead to PDZK1 phosphorylation, thus controlling SR-BI expression levels.

The phosphorylation level of PDZK1 was reduced by approximately one half when Ala was substituted for Ser-518 in ^{32}P-incorporation experiments (Fig. 3*B*). Therefore, it is possible that PDZK1 is also phosphorylated at position Ser-518. However, the Ser-509-to-Ala substitution leads to complete suppression of phosphorylation, which indicates that Ser-518 is phosphorylated after Ser-509 is phosphorylated. Whether the PDZK1 C-terminal region has other phosphorylation sites besides the Ser-509 location remains to be determined.

Glucagon, being a major regulator of plasma glucose concentration (33), has an important role in carbohydrate metabolism. The effects of glucagon are mediated by the cAMP second-messenger system, including PKA. Glucagon also influences cholesterol metabolism. Conditions with increased glucagon levels are associated with reduced plasma cholesterol levels (34, 35), and the administration of glucagon to laboratory animals as well as humans decreases plasma cholesterol levels (25–28). However, the physiological role of this phenomenon remains unclear. Glucagon has been shown to increase the number of hepatic low-density lipoprotein (LDL) receptors and concomitantly decrease plasma cholesterol and apoprotein B levels (28). According to ref. 28, the plasma HDL cholesterol level was decreased also by glucagons treatment, as we observed in this study (Fig. 7*A*). Our results show that glucagon increases expression of the HDL receptor SR-BI in

the liver. Overexpression of hepatic SR-BI leads to reduced plasma HDL levels (7, 8), which supports the hypothesis that increased SR-BI expression is responsible for reduced plasma HDL levels. Furthermore, glucagon was shown to enhance cholesterol uptake into bile in rats (36). HDL cholesterol is known to be a major substrate source for bile acid production in both rats and humans (37). Overexpression of SR-BI markedly promotes the hepatic uptake of HDL cholesterol, thus facilitating the secretion of cholesterol into bile (7, 10). One explanation for our results is that glucagon administration to rats leads to enhanced PDZK1 phosphorylation via PKA, which subsequently leads to enhanced SR-BI protein expression, regulated at a posttranscriptional level. However, it cannot yet be proven that the phosphorylation of PDZK1 leads to the described SR-BI elevation because glucagon treatment leads not only to an elevation of SR-BI but simultaneously to a 2-fold elevation of PDZK1, respectively. Use of mouse models such as PDZK1 knockout mice and SR-BI knockout mice, as well as transgenic animals expressing only the PDZK1 mutant where Ser-509 is substituted by Ala, would bring us further toward solving this problem.

In conclusion, we demonstrated in this study that phosphorylation of the PDZK1 C-terminal region is crucial for up-regulation of SR-BI protein expression and that PDZK1 phosphorylation is hormonally regulated. A major question that remains to be answered is how the phosphorylation of the PDZK1 C-terminal region is involved in the up-regulation of SR-BI levels.

1. Gordon, D. J. & Rifkind, B. M. (1989) *N. Engl. J. Med.* **321,** 1311–1316.
2. Barter, P. J. & Rye, K. A. (1996) *Atherosclerosis* **121,** 1–12.
3. Fielding, C. J. & Fielding, P. E. (1995) *J. Lipid Res.* **36,** 211–228.
4. Wang, M. & Briggs, M. R. (2004) *Chem. Rev.* **104,** 119–137.
5. Trigatti, B., Rigotti, A. & Krieger, M. (2000) *Curr. Opin. Lipidol.* **11,** 123–131.
6. Rigotti, A., Miettinen, H. E. & Krieger, M. (2003) *Endocr. Rev.* **24,** 357–387.
7. Kozarsky, K. F., Donahee, M. H., Rigotti, A., Iqbal, S. N., Edelman, E. R. & Krieger, M. (1997) *Nature* **387,** 414–417.
8. Wang, N., Arai, T., Ji, Y., Rinninger, F. & Tall, A. R. (1998) *J. Biol. Chem.* **273,** 32920–32926.
9. Ueda, Y., Royer, L., Gong, E., Zhang, J., Cooper, P. N., Francone, O. & Rubin, E. M. (1999) *J. Biol. Chem.* **274,** 7165–7171.
10. Ji, Y., Wang, N., Ramakrishnan, R., Sehayek, E., Huszar, D., Breslow, J. L. & Tall, A. R. (1999) *J. Biol. Chem.* **274,** 33398–33402.
11. Rigotti, A., Trigatti, B. L., Penman, M., Rayburn, H., Herz, J. & Krieger, M. (1997) *Proc. Natl. Acad. Sci. USA* **94,** 12610–12615.
12. Varban, M. L., Rinninger, F., Wang, N., Fairchild-Huntress, V., Dunmore, J. H., Fang, Q., Gosselin, M. L., Dixon, K. L., Deeds, J. D., Acton, S. L., *et al.* (1998) *Proc. Natl. Acad. Sci. USA* **95,** 4619–4624.
13. Mardones, P., Quinones, V., Amigo, L., Moreno, M., Miquel, J. F., Schwarz, M., Miettinen, H. E., Trigatti, B., Krieger, M., VanPatten, S., *et al.* (2001) *J. Lipid Res.* **42,** 170–180.
14. Ikemoto, M., Arai, H., Feng, D., Tanaka, K., Aoki, J., Dohmae, N., Takio, K., Adachi, H., Tsujimoto, M. & Inoue, K. (2000) *Proc. Natl. Acad. Sci. USA* **97,** 6538–6543.
15. Kocher, O., Comella, N., Tognazzi, K. & Brown, L. F. (1998) *Lab. Invest.* **78,** 117–125.
16. Wang, S., Yue, H., Derin, R. B., Guggino, W. B. & Li, M. (2000) *Cell* **103,** 169–179.
17. Kocher, O., Comella, N., Gilchrist, A., Pal, R., Tognazzi, K., Brown, L. F. & Knoll, J. H. (1999) *Lab. Invest.* **79,** 1161–1170.
18. Gentzsch, M., Cui, L., Mengos, A., Chang, X. B., Chen, J. H. & Riordan, J. R. (2003) *J. Biol. Chem.* **278,** 6440–6449.
19. Gisler, S. M., Stagljar, I., Traebert, M., Bacic, D., Biber, J. & Murer, H. (2001) *J. Biol. Chem.* **276,** 9206–9213.
20. Gisler, S. M., Pribanic, S., Bacic, D., Forrer, P., Gantenbein, A., Sabourin, L. A., Tsuji, A., Zhao, Z. S., Manser, E., Biber, J. & Murer, H. (2003) *Kidney Int.* **64,** 1733–1745.
21. Custer, M., Spindler, B., Verrey, F., Murer, H. & Biber, J. (1997) *Am. J. Physiol.* **273,** F801–F806.
22. Kocher, O., Pal, R., Roberts, M., Cirovic, C. & Gilchrist, A. (2003) *Mol. Cell. Biol.* **23,** 1175–1180.
23. Kocher, O., Yesilaltay, A., Cirovic, C., Pal, R., Rigotti, A. & Krieger, M. (2003) *J. Biol. Chem.* **278,** 52820–52825.
24. Pinna, L. A. & Ruzzene, M. (1996) *Biochim. Biophys. Acta* **1314,** 191–225.
25. Amatuzio, D. S., Grande, F. & Wada, S. (1962) *Metabolism* **11,** 1240–1249.
26. Eaton, R. P. (1973) *J. Lipid Res.* **14,** 312–318.
27. Guettet, C., Rostaqui, N., Mathe, D., Lecuyer, B., Navarro, N. & Jacotot, B. (1991) *Lipids* **26,** 451–458.
28. Rudling, M. & Angelin, B. (1993) *J. Clin. Invest.* **91,** 2796–2805.
29. Gisler, S. M., Madjdpour, C., Bacic, D., Pribanic, S., Taylor, S. S., Biber, J. & Murer, H. (2003) *Kidney Int.* **64,** 1746–1754.
30. Huang, L. J., Durick, K., Weiner, J. A., Chun, J. & Taylor, S. S. (1997) *Proc. Natl. Acad. Sci. USA* **94,** 11184–11189.
31. Burnett, P. E., Blackshaw, S., Lai, M. M., Qureshi, I. A., Burnett, A. F., Sabatini, D. M. & Snyder, S. H. (1998) *Proc. Natl. Acad. Sci. USA* **95,** 8351–8356.
32. Nemenoff, R. A., Gunsalus, J. R. & Avruch, J. (1986) *Arch. Biochem. Biophys.* **245,** 196–203.
33. Unger, R. H. (1983) *Diabetes* **32,** 575–583.
34. Vaughan, G. M., Becker, R. A., Unger, R. H., Ziegler, M. G., Siler-Khodr, T. M., Pruitt, B. A., Jr., & Mason, A. D., Jr. (1985) *Metabolism* **34,** 637–641.
35. Knapp, M. L., al-Sheibani, S. & Riches, P. G. (1991) *Clin. Chem.* **37,** 2093–2101.
36. Guettet, C., Mathe, D., Riottot, M. & Lutton, C. (1988) *Biochim. Biophys. Acta* **963,** 215–223.
37. Botham, K. M. & Bravo, E. (1995) *Prog. Lipid Res.* **34,** 71–97.

Pharmaceutical Research, Vol. 22, No. 2, February 2005 (© 2005)
DOI: 10.1007/s01869-005-1869-8

Research Paper

Estimation of the Three-Dimensional Pharmacophore of Ligands for Rat Multidrug-Resistance–Associated Protein 2 Using Ligand-Based Drug Design Techniques

Shuichi Hirono,[1,3] Izumi Nakagome,[1] Rie Imai,[1] Kazuya Maeda,[2] Hiroyuki Kusuhara,[2] and Yuichi Sugiyama[2]

Received March 22, 2004; accepted July 19, 2004

Purpose. Multidrug-resistance–associated protein 2 (Mrp2) shows a broad substrate specificity toward amphiphilic organic anions. This study identified key functional groups of ligand molecules for binding to rat Mrp2, determined their relative locations, and examined substrate specificity through receptor mapping using three-dimensional (3D) quantitative structure-activity relationship (3D-QSAR) analysis.
Methods. Ligand-binding conformations were estimated using conformational analysis (CAMDAS) and molecular superposition (SUPERPOSE) methods to clarify the substrate specificity of rat Mrp2 in relation to 3D ligand structures.
Results. Two types of binding conformations of ligands for rat Mrp2 were identified. 3D-QSAR comparative molecular-field analysis (CoMFA) revealed a statistically significant model for one type, in which the steric, electrostatic, and log P contributions to the binding affinity for rat Mrp2 were 63.0%, 33.4%, and 3.6%, respectively ($n = 16$, $q^2 = 0.59$, $n = 3$, $r^2 = 0.99$, and $s = 0.08$).
Conclusions. The 3D pharmacophore of ligands for rat Mrp2, and the ligand-binding region of rat Mrp2, were estimated. Ligand recognition of rat Mrp2 is achieved through interactions in two hydrophobic and two electrostatically positive sites (primary binding sites). The broad substrate specificity of rat Mrp2 might result from the combination of secondary (two electrostatically positive and two electrostatically negative sites) and primary binding sites.

KEY WORDS: binding conformation; 3D pharmacophore; 3D-QSAR; rat Mrp2; substrate specificity.

INTRODUCTION

The liver is one of the most important organs in the detoxification of xenobiotics, and biliary excretion is a major pathway for their elimination. Compounds in the circulating blood are taken up by hepatocytes and are then metabolized and/or excreted into the bile. Many kinds of drugs and their metabolites are transported across the sinusoidal and bile canalicular membranes via carriers. The mechanism of transport across the bile canalicular membrane has been characterized using isolated canalicular membrane vesicles (CMVs), which revealed that several types of primary active transporters are responsible for ligand efflux from the hepatocytes into the bile. Among them, multidrug-resistance–associated protein-2 (Mrp2; gene symbol ABCC2) has an important role in the biliary excretion of many organic anions and glutathione or glucuronide conjugates (1–3).

Mrp2 is an ATP-binding cassette (ABC) transporter, which possesses two highly conserved ABC regions. The Eisai hyperbilirubinemic rat (EHBR), which has a hereditary Mrp2 deficiency owing to the insertion of a nonsense mutation (4), and the GY/TR⁻ rat (5) have both helped to reveal the importance of Mrp2 in the biliary excretion of various types of organic anions. In the EHBR, the biliary excretion of Mrp2 substrates is drastically decreased, and the ATP-dependent uptake of Mrp2 substrates into CMVs prepared from EHBRs is greatly reduced compared with those prepared from normal rats.

These findings demonstrate that a wide range of organic anions can be substrates for Mrp2, which include: nonconjugated organic anions such as dibromosulfophthalein (6,7), cefodizime (β-lactam antibiotic) (7), pravastatin (a 3-hydroxy-3-methyl-glutaryl-coenzyme A reductase inhibitor) (8), temocaprilat (an angiotensin-converting enzyme inhibitor) (9), the carboxylate forms of CPT-11 and its active metabolite (SN-38, which is a topoisomerase inhibitor) (8), and a cyclic anionic peptide (BQ-123, which is an endothelin antagonist) (10); glutathione conjugates such as leukotriene C_4 (11) and DNP-SG (12); and glucuronide conjugates such as bilirubin glucuronide (13), E3040 glucuronide (14,15), and SN-38 glucuronide (16).

[1] School of Pharmaceutical Sciences, Kitasato University, Tokyo 108-8641, Japan.
[2] Graduate School of Pharmaceutical Sciences, University of Tokyo, Tokyo 113-0033, Japan.
[3] To whom correspondence should be addressed. (e-mail: hironos@pharm.kitasato-u.ac.jp)

ABBREVIATIONS: ABC, ATP-binding cassette; CAMDAS, Conformational Analyzer with Molecular Dynamics and Sampling; C log P, calculated log P; CMVs, canalicular membrane vesicles; CoMFA, comparative molecular-field analysis; EHBR, Eisai hyperbilirubinemic rat; MD, molecular dynamics; Mrp2, multidrug-resistance-associated protein 2; PLS, partial least squares; QSAR, quantitative structure-activity relationship; rmsd, root-mean-square deviation; SD, Sprague-Dawley.

Clearly, rat Mrp2 accepts many organic anions as substrates. However, its broad substrate specificity has not been investigated in terms of the three-dimensional (3D) structures of ligands (17), and the complete 3D structure has not been determined for any mammalian transporter. Elucidating the structural characteristics of the ligand-binding region of rat Mrp2 would be useful for understanding its broad substrate specificity. Therefore, in the current study, we investigated the binding conformation of ligands to rat Mrp2, the key functional groups for binding to Mrp2 (3D pharmacophore), and the 3D quantitative structure-activity relationships (3D-QSAR) between ligands and rat Mrp2. Our combined method comprised the following three procedures: first, conformational analysis (CAMDAS) (18); second, a molecular superposition procedure (SUPERPOSE) (19); and third, 3D-QSAR analysis by comparative molecular-field analysis (CoMFA) (20). These techniques are described in more detail in the following section.

MATERIALS AND METHODS

Conformational Analysis: Sampling of a Set of Conformers of a Molecule

X-ray structural analysis of protein-ligand complexes has revealed that the binding conformation is one of the stable conformations of a ligand molecule. To generate a set of conformers of ligands, we used the automated program Conformational Analyzer with Molecular Dynamics and Sampling (CAMDAS), which was developed by Tsujishita and Hirono (18). CAMDAS performs high-temperature molecular dynamics (MD) calculations for a target molecule and for sampled conformers that appear during the MD. It then evaluates the similarities between each of the sampled conformers in terms of dihedral angle values, clusters similar conformers together, and, finally, prints out the clustered conformers. In this way, CAMDAS can find the representative conformers from an arbitrarily given structure of the molecule.

To estimate the binding conformation of ligands to rat Mrp2, MD dynamics calculations were executed for 18 ligands (a training set for constructing QSAR models comprising compounds **1–16** and a test set for verifying the QSAR models comprising compounds **A** and **B**), and many conformers were sampled; their chemical structures are shown in Figs. 1 and 2. An MD calculation for sampling was performed for 800 ps with an integral time step of 0.001 ps using an MM2 force field (21) without electrostatic and hydrogen-bonding interactions. The temperature of the system was maintained at 1200 K, and the length of the covalent bonds was fixed using the SHAKE algorithm throughout the MD simulations. Conformers were sampled at every 100 steps and preclustered with dihedral angles during the MD simulations. If the difference between conformers was within ±30°, they were grouped together. Subsequently, reclustering of the sampled conform-

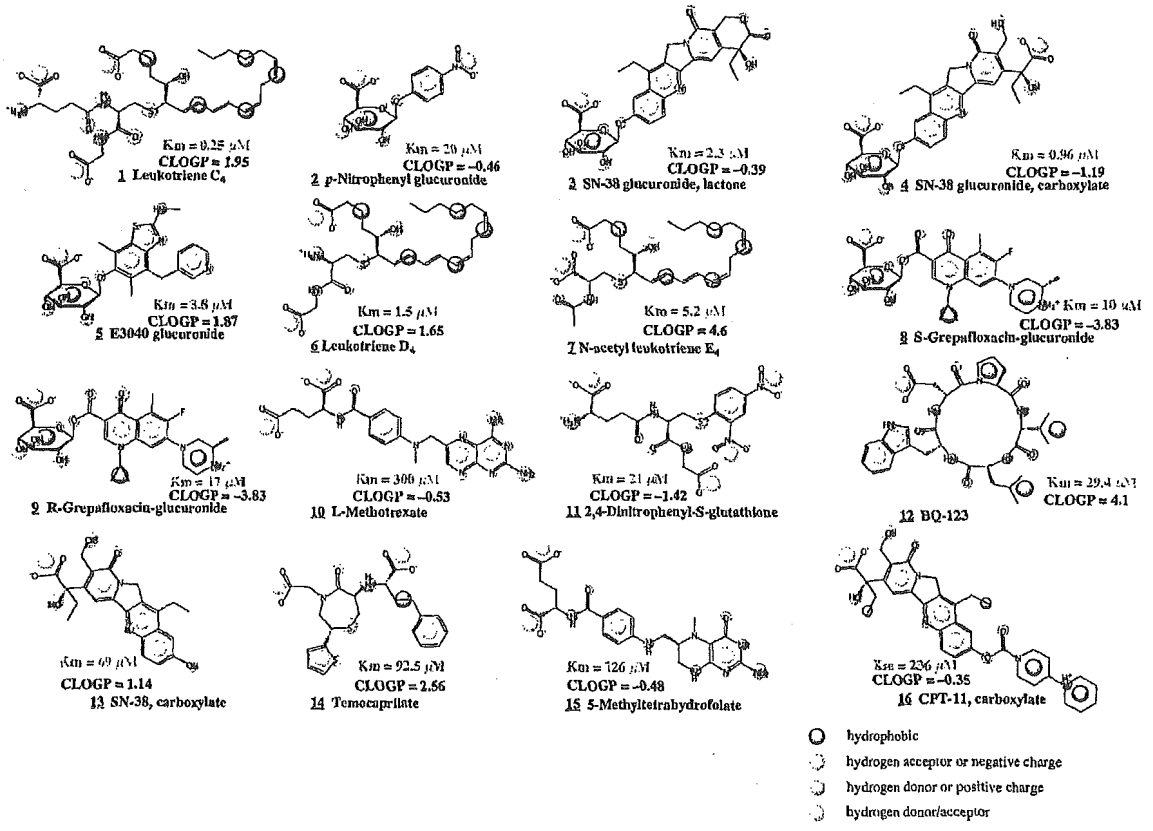

Fig. 1. Chemical structures of the compounds in the training set, with property spheres, K_m, and C log P values.

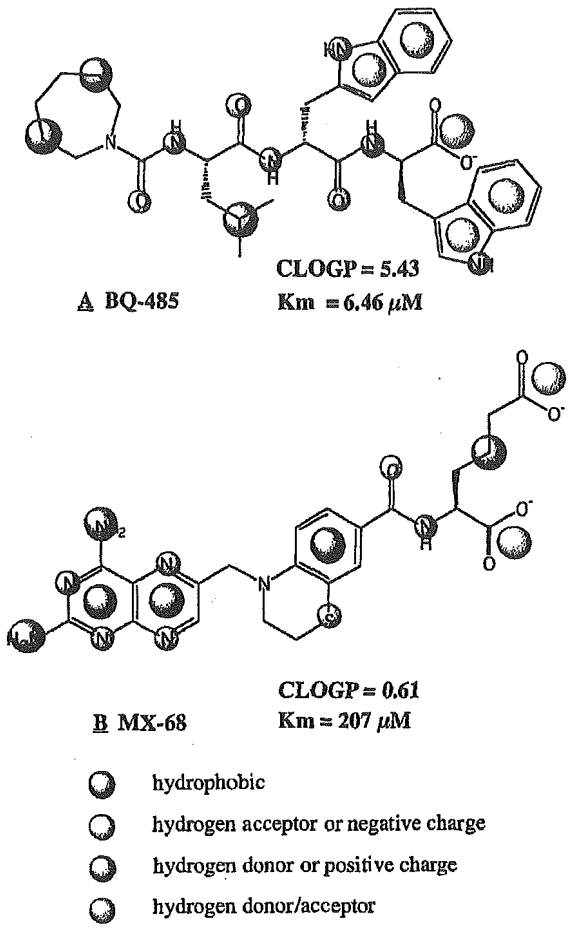

Fig. 2. Chemical structures of the compounds in the test set, with property spheres, K_m, and C log P values.

ers was performed with dihedral angles within ±30°. Before the clustering, each conformer was minimized until the root-mean-square (rms) of the gradients of the potential energy was below 0.004 kcal mol^{-1} $Å^{-1}$.

Molecular Superposition: Selection of the Candidate Binding Conformations

X-ray crystallographic studies of protein-ligand complexes have demonstrated that when ligands bind to a given protein, such as a receptor or a transporter, the atomic groups in the ligands that interact with amino-acid residues of the protein occupy the same 3D space. Based on this information, we carried out molecular superposition for ligand molecules using the SUPERPOSE program developed by Iwase and Hirono (19). The program superposes two molecules based on the physicochemical properties of the atomic groups, which is useful for elucidating a pharmacophore and estimating a binding conformation by distinguishing it from among the many conformations that are generated by high-temperature MD calculations.

Five types of physicochemical properties are considered in the program, including hydrophobic (aromatic), hydrogen-bond donors, hydrogen-bond acceptors, and hydrogen-bond donors/acceptor. Each type is represented as a sphere with a predefined radius and is assigned to a functional group in a molecule. After molecular superposition, the overlaps of the spheres are scored.

The program works as follows. First, a large molecule with its physicochemical properties represented by spheres is fixed at the center of a large box, and another smaller molecule, also with spheres representing its physicochemical properties, is translated and rotated in the box. The translational increment is 1 Å, and the center of mass is translated onto the body-centered-cubic lattice-points made in the circumscribed large-volume rectangular box. The rotation is performed on each of the lattice points. The ranges of the three Eulerian angles are $0° \leq \phi, \varphi < 360°$, and $0° \leq \theta \leq 180°$. The rotational increment is 4°. Second, at every translation or rotation, the property spheres that overlap are determined by calculating the distances between the spheres of the molecules. Third, overlaps of the spheres are scored so that points are added when atomic groups with the same physicochemical properties overlap, and points are subtracted when atomic groups with different physicochemical properties overlap, according to the scoring table (19). Atomic groups without overlaps are not scored.

These three operations are repeated to determine the orientation with the highest score and the smallest rms deviation (rmsd) of the distances of the overlapped atomic groups between the two molecules.

3D-QSAR Analyses: Determination of the Binding Conformation Using CoMFA

The SUPERPOSE program identified several plausible binding conformations. We therefore carried out comparative molecular field analysis (CoMFA) to determine the binding conformation of ligands to rat Mrp2 and to obtain 3D structure-activity relationships.

Table I. Results of Conformational Analysis by CAMDAS

	Number of conformers	ΔE (kcal/mol)	Number of conformers within 12 kcal/mol
Training set			
1	7777	15.570	3846
2	16	14.406	15
3	262	18.565	234
4	876	18.877	798
5	251	16.972	240
6	7777	13.951	5723
7	3121	1112.579	1576
8	479	54.432	316
9	264	32.593	180
10	2547	1013.488	2387
11	3957	978.039	3530
12	5937	53.872	1533
13	177	13.669	176
14	3078	52.334	2832
15	3069	1028.764	2915
16	5135	32.084	3856
Test set			
A	36	480.492	20
B	7777	86.823	4966

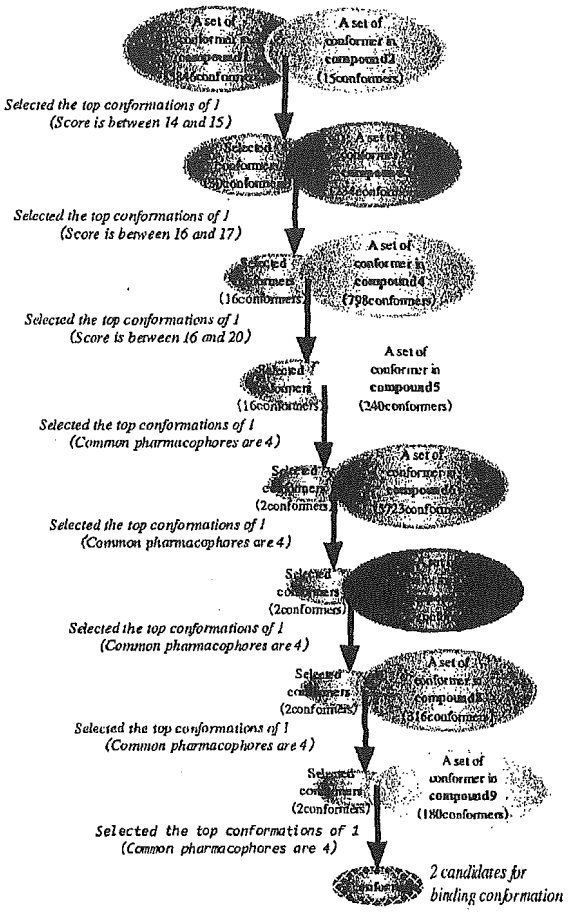

Fig. 3. Flowchart of SUPERPOSE.

The atomic charges of each conformer were calculated using the semiempirical molecular orbital program package MOPAC93 MNDO/ESP, in order to evaluate the electrostatic field in CoMFA. Conventional CoMFA was performed using the QSAR option of SYBYL (Tripos, Inc., St. Louis, MO, USA), with the Michaelis constant (K_m) (22) of each ligand included as bioactive data, as shown in Figs. 1 (training set) and 2 (test set). For the K_m-determination experiments, CMVs were prepared from male Sprague-Dawley (SD) rats, and the transport study was performed using the rapid-filtration technique, as described previously (11,12). All of the compounds were mainly excreted into the bile via rat Mrp2, as biliary excretion in EHBRs and/or the ATP-dependent uptake of each compound into CMVs prepared from EHBRs was disrupted. Therefore, the K_m values for the uptake into CMVs prepared from SD rats corresponded to those for rat Mrp2.

Two calculations were carried out, using an sp^3 carbon probe atom with a charge of +1 and either the steric and electrostatic components or the steric, electrostatic, and calculated log P (C log P) components. The calculated values of log P were estimated using the CLOGP program (Daylight, C.I.S. Inc., Rochester, NY, USA). The CoMFA QSAR equations were calculated with the partial least squares (PLS) algorithm. The optimal number of components in the final CoMFA PLS model was determined using the cross-validated R^2 (q^2) values obtained from the leave-one-out cross-validation technique. The CoMFA PLS model with the highest q^2 values was selected to estimate the binding conformation of ligands for rat Mrp2.

RESULTS

Sampling of a Set of Conformers of Each Ligand

Using the CAMDAS program, we carried out conformational analyses of ligand molecules bound to rat Mrp2. The high-temperature MD calculation was used with a potential function without an electrostatic interaction term and a hydrogen-bonding term to avoid undesirable intramolecular interactions (Figs. 1 and 2). The CAMDAS calculations gave many conformers of the 18 compounds, as shown in Table I. The sets of conformers of compounds **1–9**, the structures of which were significantly different from one another and showed relatively low K_m values, were used by the SUPERPOSE

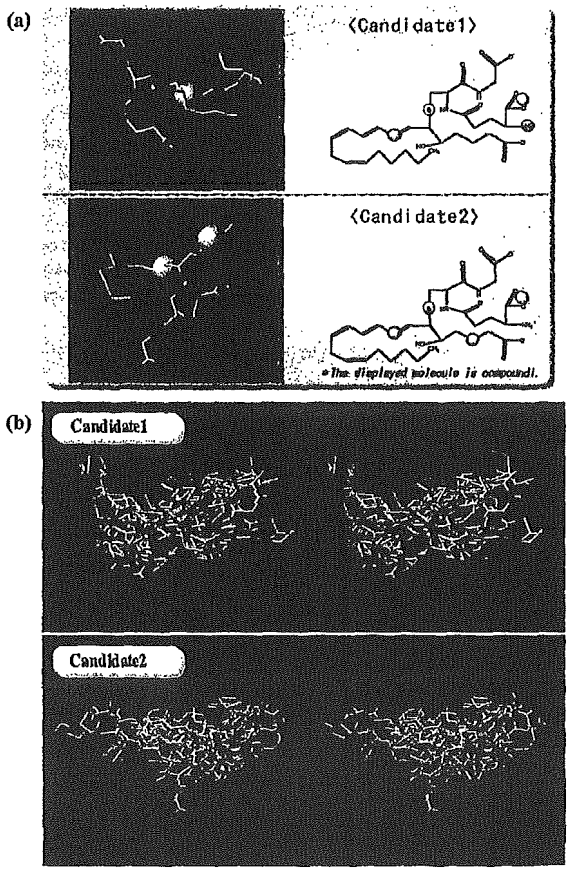

Fig. 4. (a) Property spheres common to compounds **1–9**. (b) Stereo views of superposed compounds in the training set (yellow molecule: compound **1**).

Table II. Results of CoMFA

Field type		Candidate 1		Candidate 2	
		ST + EL	ST + EL + C log P	ST + EL	ST + EL + C log P
Cross-validated	q^2	0.03	0.01	0.36	0.59
	s_{press}	1.21	1.15	0.80	0.64
No. of components		7	6	3	3
Conventional	r^2	1.00	1.00	0.99	0.99
	F	30122.14	2114.33	485.66	613.30
	s	0.01	0.03	0.09	0.08
Contribution (%)	ST	56.6	53.1	60.2	63.0
	EL	43.4	40.5	39.8	33.4
	C log P[a]	—	6.4	—	3.6

St, steric field; EL, electrostatic field; CoMFA, comparative molecular-field analysis.
[a] log P calculated by CLOGP.

program to determine the 3D pharmacophore of the ligand and to obtain the candidate binding conformations.

Selection of Candidate Binding Conformations

As shown in Table I, relatively stable conformers with molecular energies within 12 kcal/mol from the global minimum were selected as the conformers to be superposed. The cutoff value of 12 kcal/mol was confirmed in our previous study (19). For each ligand, the atomic groups that the property spheres were assigned to are shown in Figs. 1 (training set) and 2 (test set).

Initially, 3846 conformers of compound **1** and 15 conformers of compound **2** were superposed (Fig. 3). Each overlap was ranked on the basis of the SUPERPOSE score and the rmsd. As a result, we selected 30 conformers of compound **1** that represented good overlaps, with scores ranging between 14 and 15. Next, these 30 conformers of compound **1** and 234 conformers of compound **3** were superposed. As a result, we selected 16 conformers of compound **1** that showed good overlaps with conformers of compound **3**, with scores ranging between 16 and 17. The 16 selected conformers of compound **1** were then superposed to 798 conformers of compound **4**. No change was observed in the number of good overlaps at this stage, with scores ranging between 16 and 20 for all of the conformers. All 16 conformers of compound **1** were therefore superposed with 240 conformers of compound **5**. There were only two good overlaps for the superposition of compound **1** with compound **5**, with four commonly overlapped functional groups. Using the same method, the selected conformers of compound **1** were superposed to conformers of compounds **6–9** (Fig. 3). We finally obtained two conformers of compound **1** that were considered to be good candidates for the binding conformation. Figure 4a shows the common property spheres; namely, the pharmacophores obtained by superposition using compounds **1–9**.

Next, each candidate for the binding conformation was superposed to conformers of compounds **10–16** in the training set. The atomic groups that the ligand property spheres were assigned to are shown in Fig. 1. In this way, candidate binding conformations of compounds **10–16** were obtained. We then estimated the molecular alignment of ligand molecules (compounds **1–16**) that were essential to CoMFA (Fig. 4b). The

Table III. The Values of $\log(1/K_m)$ Calculated Using the Final CoMFA QSAR Model Compared with Experimental Data

	Experimental	Calculated	Residual
Compounds in the training set			
1 Leukotriene C4	6.60	6.70	−0.10
2 *p*-Nitrophenyl glucuronide	4.70	4.60	0.10
3 SN-38 glucuronide, lactone	5.64	5.63	0.01
4 SN-38 glucuronide, carboxylate	6.02	5.90	0.12
5 E3040 glucuronide	5.42	5.36	0.06
6 Leukotriene D4	5.82	5.77	0.05
7 *N*-acetyl leukotriene E4	5.28	5.33	−0.05
8 (*S*)-Grepafloxacin-glucuronide	5.00	5.00	0.00
9 (*R*)-Grepafloxacin-glucuronide	4.77	4.83	−0.06
10 L-Methotrexate	3.52	3.47	0.05
11 2,4-Dinitrophenyl-*S*-glutathione	4.68	4.76	−0.08
12 BQ-123	4.53	4.46	0.07
13 SN-38, carboxylate	4.16	4.25	−0.09
14 Temocaprilate	4.03	4.09	−0.06
15 5-Methyltetrahydrofolate	3.90	3.84	0.06
16 CPT-11, carboxylate	3.63	3.69	−0.06
Compounds in the test set			
A BQ-485	5.19	5.10	0.09
B MX-68	3.68	4.16	−0.48

two candidates of binding conformation of ligands for rat Mrp2 generated two types of molecular alignments, as shown in Fig. 4b. We also obtained binding conformation candidates for compounds **A–B** for the test set using a similar method to the training set. The test set was used to evaluate the predictive power of the CoMFA model obtained using the training set.

Determination of the Binding Conformation by CoMFA

CoMFA calculations were carried out using the two molecular alignments. The atomic charges of each conformer were calculated using MOPAC93 MNDO/ESP to evaluate the electrostatic field in CoMFA. Conventional CoMFA was performed with the QSAR option of SYBYL. For each molecular alignment (candidate 1 and candidate 2), two types of calculations were carried out together with an sp^3 carbon probe atom with a +1 charge: the first used steric and electrostatic fields, and the second used steric and electrostatic fields along with calculated values of log P (C log P). The CoMFA QSAR equations were calculated with the PLS algorithm. The optimal number of components in the final CoMFA PLS model was determined using the cross-validated R^2 (q^2) values obtained by the leave-one-out technique. The cross-validated R^2 (q^2) values, the standard error of the predictive sum of squares (s_{press}), and the standard error of the estimate (r^2) are listed in Table II for each candidate. The CoMFA PLS model with the highest q^2 values was assumed to best explain the binding conformation.

A good CoMFA model with three PLS components was obtained using the steric and electrostatic fields along with C log P for candidate 2. The final CoMFA model had a q^2 value of 0.59 with six PLS components, an s_{press} value of 0.64, an r^2 value of 0.99, and a standard error of 0.08. The experimental and calculated values of $\log(1/K_m)$ for each compound in the training set are listed in Table III. The property spheres shown in Fig. 5 illustrate the important atomic groups for the binding of each ligand molecule to rat Mrp2.

We also investigated the predictivity of the final CoMFA model using the test set of compounds. The values of $\log(1/K_m)$ calculated using the CoMFA model of candidate 2 with the steric field, electrostatic field, and C log P showed good agreement with the experimental values (Table III). We therefore concluded that the 3D structure of candidate 2 reflects the binding conformation of ligands for rat Mrp2. In the test set, the calculated value of $\log(1/K_m)$ for BQ-485 (5.10) compared well with the experimental value (5.19), whereas the calculated value of MX-68 contained a larger error (0.48). This might be the result of the difficulties of determining the atomic charges of MX-68, which has a pteridine ring, using MOPAC93 MNDO/ESP.

Figure 6a shows a contour map of the steric field from the final CoMFA model, together with the binding conformation of compound **1**: the green contours indicate areas in which bulky atomic groups are sterically favorable for the binding affinity, and the yellow contours indicate areas in which bulky groups are unfavorable for the binding affinity. Figure 6b shows a contour

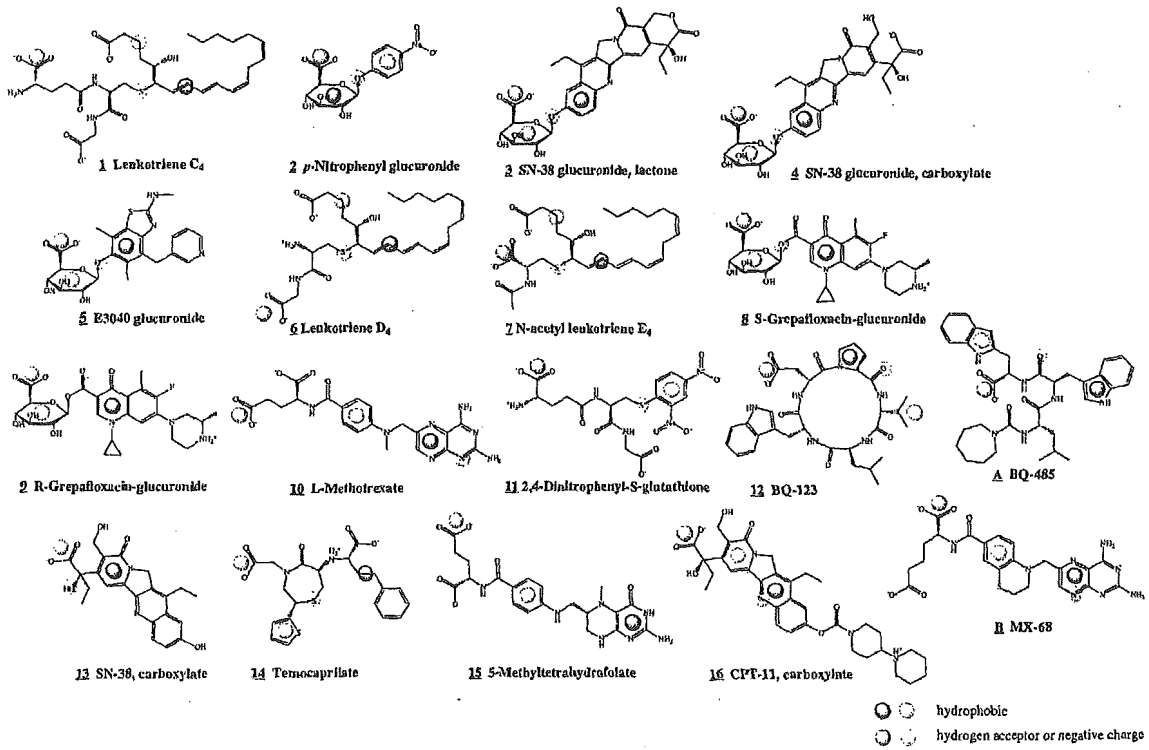

Fig. 5. Atomic groups involved in the binding of each ligand molecule to Mrp2/ABCC2.

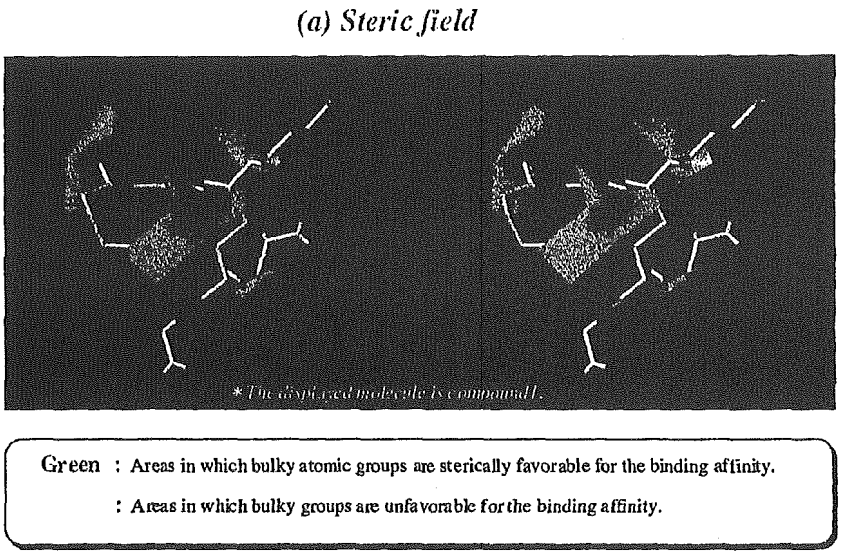

Fig. 6. Stereo views of contour maps obtained from the final CoMFA model. (a) Steric field. (b) Electrostatic field.

map of the electrostatic field from the final CoMFA model, together with the binding conformation of compound **1**; the blue contours indicate areas in which atomic groups with positive charges are advantageous to the binding of ligand with rat Mrp2, and the red contours show areas in which atomic groups with negative charges are favorable for the binding of ligand with rat Mrp2. The areas shown in the contour map are of great importance for explaining variation in the binding affinities of ligands with rat Mrp2.

DISCUSSION

Pharmacophore of Ligands for Rat Mrp2

We have identified a plausible binding conformation of ligands to rat Mrp2 by making full use of ligand-based drug design techniques. In this conformation, four property spheres that are common to all ligands were identified using the SUPERPOSE calculation. We propose that the spatial arrangement of the four functional groups expressed by these property spheres represents a 3D pharmacophore of ligands for rat Mrp2. Figure 7 shows a stereo view of these four property spheres along with the 3D structure of compound **1** and its structural formula. It appears that two hydrogen bond-acceptor groups (HA1 and HA2) and two hydrophobic groups (HP1 and HP2) are essential for the binding of ligands to rat Mrp2 and that these groups constitute the 3D pharmacophore. Figure 8 shows the relative distances between the four property spheres that represent the essential functional groups for ligand binding. The distances are as follows: HA1–HA2, ~5.0 &ARING;; HA1–HP1, ~5.3 &ARING;; HA1–

HP2, ~5.5 &ARING;; HA2–HP1, 4.7 &ARING;; HA2–HP2, 3.2 &ARING;; and HP1–HP2, 4.8 &ARING;.

Estimation of the Ligand-Binding Site of Rat Mrp2

A good CoMFA model was identified with the following parameters: a q^2 value of 0.59 with six PLS components, an s_{press} value of 0.64, an r^2 value of 0.99, and a standard error of 0.08. We suggest that the success of the CoMFA was a result of the use of the molecular alignment obtained using SUPERPOSE. This represents a unique and distinctive approach, in which the binding conformation and 3D pharmacophore of a ligand are estimated using ligand-based drug design techniques and are then applied to the molecular alignment, which is essential to CoMFA.

On the basis of the 3D pharmacophore and the contour map obtained from the CoMFA calculation, we have estimated the structure of the ligand-binding site of rat Mrp2 (Fig. 9). The four primary binding sites correspond to the 3D pharmacophore, comprising the four functional groups that are essential for the binding of ligands to rat Mrp2. The model also suggests that secondary binding sites, which correspond to specific contour levels in the CoMFA contour map, are important in explaining the variation of the binding affinities of ligands to rat Mrp2.

In conclusion, we propose that both hydrophobic and electrostatic interactions have vital roles in the binding of ligands to rat Mrp2. Ligand recognition seems to be achieved through interactions in the two hydrophobic sites and the two electrostatically positive sites (primary binding sites). Moreover, the broad substrate specificity of rat Mrp2 might be achieved by combinations of the secondary binding sites (two electrostatically positive sites and two electrostatically negative sites) with the primary binding sites.

The method described here for determining the binding conformation of ligands represents a powerful tool in cases where ligands have the same binding mode to the target protein. Of course, it should be noted that different binding modes might exist for some ligands; however, all of the ligands used in this analysis appeared to have the same binding mode, according to the results of the CoMFA. We believe that our data will be useful in the development of new com-

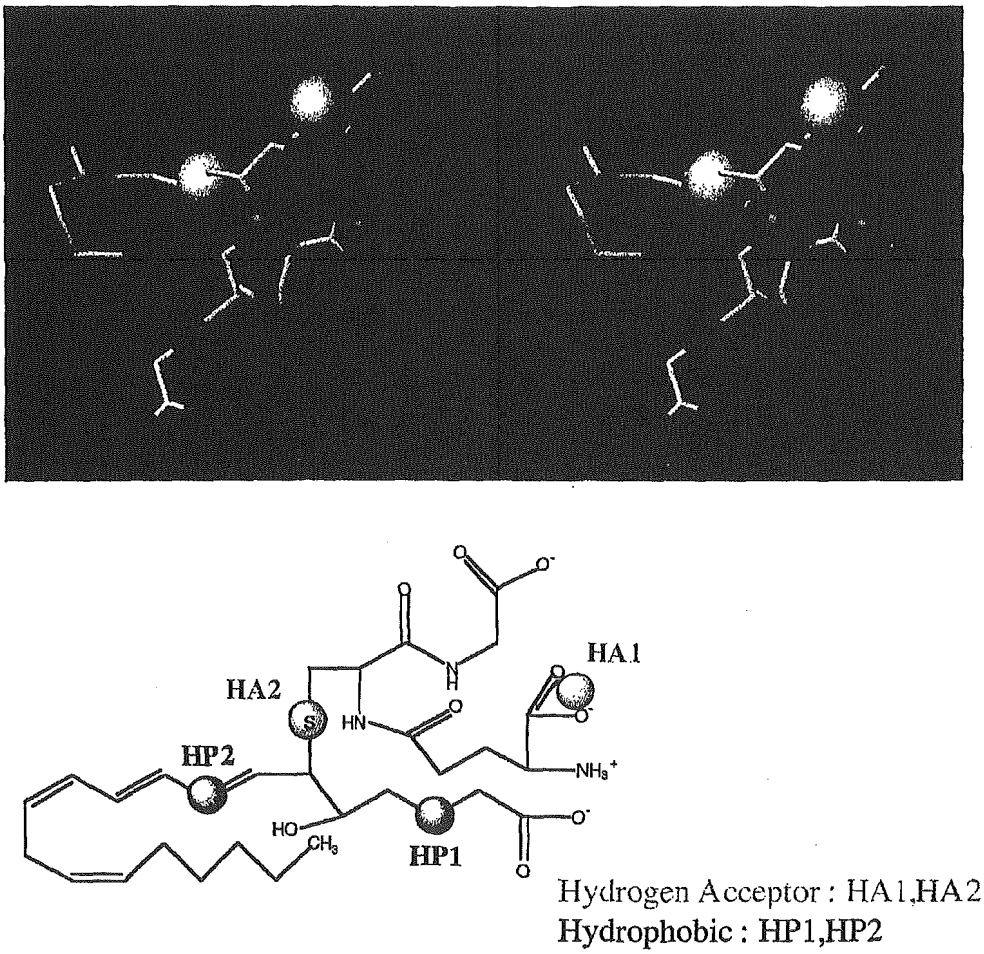

Fig. 7. A stereo view of the four property spheres that represent a 3D pharmacophore of ligands for Mrp2/ABCC2 and the 3D structure of compound 1 together with its structural formula.

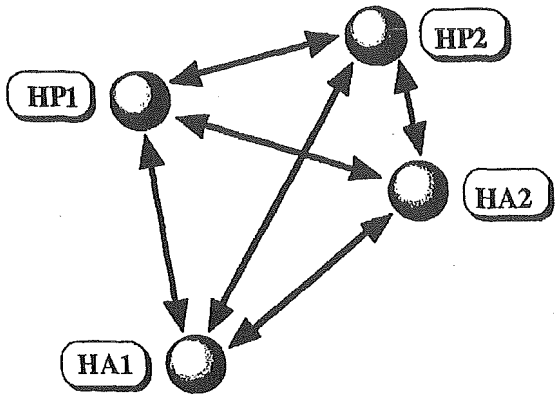

	Relative distances (Å)
HA1 - HA2	5.0 ± 0.9
HA1 - HP1	5.3 ± 0.7
HA1 - HP2	5.5 ± 1.6
HP1 - HA2	4.7 ± 0.8
HP1 - HP2	4.8 ± 1.1
HA2 - HP2	3.2 ± 1.2

Fig. 8. Relative distances between the four property spheres representing the functional groups that are essential for ligand binding.

compounds using the CoMFA QSAR model in order to evaluate their affinity for Mrp2.

REFERENCES

1. O. R. P. Elferink, D. K. Meijer, F. Kuipers, P. L. Jansen, A. K. Groen, and G. M. Groothuis. Hepatobiliary secretion of organic compounds; molecular mechanisms of membrane transport. *Biochim. Biophys. Acta* **1241**:215–268 (1995).
2. M. Yamazaki, H. Suzuki, and Y. Sugiyama. Recent advances in carrier-mediated hepatic uptake and biliary excretion of xenobiotics. *Pharm. Res.* **13**:497–513 (1996).
3. D. Keppler and J. Konig. Hepatic canalicular membrane 5: expression and localization of the conjugate export pump encoded by the *Mrp2* (*cMRP/cMOAT*) gene in liver. *FASEB J.* **11**:509–516 (1997).
4. K. Ito, H. Suzuki, T. Hirohashi, K. Kume, T. Shimizu, and Y. Sugiyama. Molecular cloning of canalicular multispecific organic anion transporter defective in EHBR. *Am. J. Physiol.* **272**:G16–G22 (1997).
5. C. C. Paulusma, P. J. Bosma, G. J. Zaman, C. T. Bakker, M. Otter, G. L. Scheffer, R. J. Scheper, P. Borst, and O. R. P. Elferink. Congenital jaundice in rats with a mutation in a multidrug resistance-associated protein gene. *Science* **271**:1126–1128 (1996).
6. K. Sathirakul, H. Suzuki, K. Yasuda, M. Hanano, O. Tagaya, T. Horie, and Y. Sugiyama. Kinetic analysis of hepatobiliary transport of organic anions in Eisai hyperbilirubinemic mutant rats. *J. Pharmacol. Exp. Ther.* **265**:1301–1312 (1993).
7. K. Sathirakul, H. Suzuki, T. Yamada, M. Hanano, and Y. Sugiyama. Multiple transport systems for organic anions across the bile canalicular membrane. *J. Pharmacol. Exp. Ther.* **268**:65–73 (1994).
8. M. Yamazaki, S. Akiyama, K. Ni'inuma, R. Nishigaki, and Y. Sugiyama. Biliary excretion of pravastatin in rats: contribution of the excretion pathway mediated by canalicular multispecific organic anion transporter. *Drug Metab. Dispos.* **25**:1123–1129 (1997).
9. H. Ishizuka, K. Konno, H. Naganuma, K. Sasahara, Y. Kawahara, K. Niinuma, H. Suzuki, and Y. Sugiyama. Temocaprilat, a novel angiotensin-converting enzyme inhibitor, is excreted in bile via an ATP-dependent active transporter (cMOAT) that is deficient in

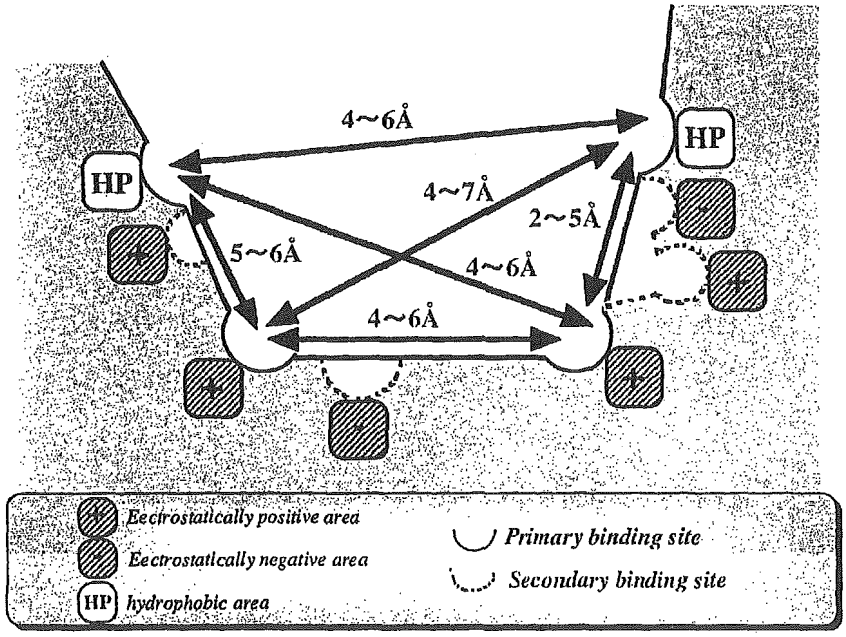

Fig. 9. Ligand-binding region of Mrp2/ABCC2 estimated using the 3D pharmacophore and CoMFA contour map.

Eisai hyperbilirubinemic mutant rats (EHBR). *J. Pharmacol. Exp. Ther.* **280**:1304–1311 (1997).
10. H. C. Shin, Y. Kato, T. Yamada, K. Niinuma, A. Hisaka, and Y. Sugiyama. Hepatobiliary transport mechanism for the cyclopentapeptide endothelin antagonist BQ-123. *Am. J. Physiol.* **272**: G979–G986 (1997).
11. T. Ishikawa, M. Muller, C. Klunemann, T. Schaub, and D. Keppler. ATP-dependent primary active transport of cysteinyl leukotrienes across liver canalicular membrane. Role of the ATP-dependent transport system for glutathione S-conjugates. *J. Biol. Chem.* **265**:19279–19286 (1990).
12. K. Kobayashi, Y. Sogame, H. Hara, and K. Hayashi. Mechanism of glutathione S-conjugate transport in canalicular and basolateral rat liver plasma membranes. *J. Biol. Chem.* **265**:7737–7741 (1990).
13. T. Nishida, Z. Gatmaitan, J. Roy-Chowdhry, and I. M. Arias. Two distinct mechanisms for bilirubin glucuronide transport by rat bile canalicular membrane vesicles. Demonstration of defective ATP-dependent transport in rats (TR-) with inherited conjugated hyperbilirubinemia. *J. Clin. Invest.* **90**:2130–2135 (1992).
14. O. Takenaka, T. Horie, K. Kobayashi, H. Suzuki, and Y. Sugiyama. Kinetic analysis of hepatobiliary transport for conjugated metabolites in the perfused liver of mutant rats (EHBR) with hereditary conjugated hyperbilirubinemia. *Pharm. Res.* **12**:1746–1755 (1995).
15. M. Trauner, M. Arrese, C. J. Soroka, M. Ananthanarayanan, T. A. Koeppel, S. F. Schlosser, F. J. Suchy, D. Keppler, and J. L. Boyer. The rat canalicular conjugate export pump (Mrp2) is down-regulated in intrahepatic and obstructive cholestasis. *Gastroenterology* **113**:255–264 (1997).
16. X. Y. Chu, Y. Kato, and Y. Sugiyama. Multiplicity of biliary excretion mechanisms for irinotecan, CPT-11, and its metabolites in rats. *Cancer Res.* **57**:1934–1938 (1997).
17. H. Suzuki and Y. Sugiyama. Role of transporters in the detoxification of xenobiotics: recent advances in the study of cMOAT/MRP. *Tanpakushitsu Kakusan Koso* **42**:1273–1284 (1997).
18. H. Tsujishita and S. Hirono. CAMDAS: an automated conformational analysis system using molecular dynamics. *J. Comput. Aided Mol. Des.* **11**:305–315 (1997).
19. K. Iwase and S. Hirono. Estimation of active conformations of drugs by a new molecular superposing procedure. *J. Comput. Aided Mol. Des.* **13**:499–512 (1999).
20. R. D. Cramer, D. E. Patterson, and J. D. Bunce. Comparative molecular field analysis (CoMFA). 1. Effect of shape on binding of steroids to carrier proteins. *J. Am. Chem. Soc.* **110**:5959–5967 (1988).
21. N. L. Allinger. Conformational analysis. 130. MM2. A hydrocarbon force field utilizing V1 and V2 torsional terms. *J. Am. Chem. Soc.* **99**:8127–8134 (1977).
22. H. Suzuki and Y. Sugiyama. Transporters for bile acids and organic anions. *Pharm. Biotechnol.* **12**:387–439 (1999).

THE JOURNAL OF BIOLOGICAL CHEMISTRY
Vol. 280, No. 2, Issue of January 14, pp. 1384–1391, 2005
Printed in U.S.A.

Use of Photoaffinity Labeling and Site-directed Mutagenesis for Identification of the Key Residue Responsible for Extraordinarily High Affinity Binding of UCN-01 in Human α1-Acid Glycoprotein*

Received for publication, September 27, 2004, and in revised form, October 26, 2004
Published, JBC Papers in Press, October 27, 2004, DOI 10.1074/jbc.M411076200

Masaaki Katsuki‡, Victor Tuan Giam Chuang‡§, Koji Nishi‡, Kohichi Kawahara¶, Hitoshi Nakayama¶, Noriyuki Yamaotsu‖, Shuichi Hirono‖, and Masaki Otagiri‡**

From the Departments of ‡Biopharmaceutics and ¶Molecular Cell Function, Graduate School of Medical and Pharmaceutical Sciences, Kumamoto University, 5-1 Oe-honmachi, Kumamoto, 862-0973, Japan, the §Department of Pharmacy, Faculty of Allied Health Sciences, Universiti Kebangsaan Malaysia, Jalan Raja Muda Abdul Aziz, 50300 Kuala Lumpur, Malaysia, and ‖The School of Pharmaceutical Sciences, Kitasato University, 5-9-1, Shirokane, Minato-ku, Tokyo, 108-8641, Japan

7-Hydroxystaurosporine (UCN-01) is a protein kinase inhibitor anticancer drug currently undergoing a phase II clinical trial. The low distribution volumes and systemic clearance of UCN-01 in human patients have been found to be caused in part by its extraordinarily high affinity binding to human α1-acid glycoprotein (hAGP). In the present study, we photolabeled hAGP with [^{3}H]UCN-01 without further chemical modification. The photolabeling specificity of [^{3}H]UCN-01 was confirmed by findings in which other hAGP binding ligands inhibited formation of covalent bonds between hAGP and [^{3}H]UCN-01. The amino acid sequence of the photolabeled peptide was concluded to be SDVVYTDXK, corresponding to residues Ser-153 to Lys-161 of hAGP. No PTH derivatives were detected at the 8th cycle, which corresponded to the 160th Trp residue. This strongly implies that Trp-160 was photolabeled by [^{3}H]UCN-01. Three recombinant hAGP mutants (W25A, W122A, and W160A) and wild-type recombinant hAGP were photolabeled by [^{3}H]UCN-01. Only mutant W160A showed a marked decrease in the extent of photoincorporation. These results strongly suggest that Trp-160 plays a prominent role in the high affinity binding of [^{3}H]UCN-01 to hAGP. A docking model of UCN-01 and hAGP around Trp-160 provided further details of the binding site topology.

Human α1-acid glycoprotein (hAGP)[1] is an acute phase protein with a molecular mass of 41 to 43 kDa and is heavily glycosylated (45%) (1). It contains sialic acids, which cause it to be negatively charged (pI = 2.7~3.2) (2). Its glycosylation pattern can change depending on the type of inflammation (3). The biological function of hAGP is not clear, although studies using *in vivo* models of inflammation indicate that it plays anti-inflammatory and immunomodulating roles and has protective effects (4, 5). The "basal" level of hAGP is ~20 μmol/liter, but hAGP levels can increase by 5–10-fold in response to stress, infection, or an inflammatory response to neoplasm (6, 7). In addition to increases in hAGP plasma concentration in certain cancers, changes in the expression of genetic variants of hAGP can occur according to the specific type of cancer (8). The levels of hAGP vary widely and heterogeneously among cancer patients; according to the type of disease, the composition of hAGP consists of various isoforms and degrees of glycosylation (9). Studies have shown that increases in circulating hAGP alter the pharmacokinetic disposition and pharmacological action of numerous drugs that bind to it (10–12). For example, increased hAGP levels associated with advanced tumors alter the pharmacokinetics of Imatinib (STI571), a tyrosine kinase inhibitor, in leukemia patients (13). hAGP also appears to be an independent predictor of response and a major objective prognostic factor of survival in patients with non-small cell lung cancer treated with docetaxel chemotherapy (14). Thus, hAGP is an important modulator of drug pharmacokinetics and pharmacodynamics in anticancer therapeutics.

7-Hydroxystaurosporine (UCN-01) has an indolocarbazole moiety and was originally isolated as a selective inhibitor of a Ca^{2+}- and phospholipid-dependent protein kinase (protein kinase C (PKC)) (15). UCN-01 is a derivative of staurosporine, which occurs naturally, inhibits numerous other kinases, and has greater selectivity for PKC than does staurosporine (16, 17). UCN-01 can mediate 3 distinct cellular effects *in vitro*: cell cycle arrest, induction of apoptosis, and potentiation of DNA damage-related toxicity (18–20). It exhibits anticancer activity against human and murine tumor cell lines that have aberrations in cellular signal transduction (21–24). Unlike other compounds with an indolocarbazole moiety, UCN-01 preferentially induces G_1 phase accumulation in various cell lines, and one of its mechanisms of action is clearly mediated by dephosphorylation of retinoblastoma protein and inhibition of cyclin-dependent kinase 2 (CDK2), an intracellular retinoblastoma protein kinase that regulates the transition from the G_1 to S phase (25). In addition, UCN-01 enhances the anticancer effects of several important chemotherapeutic drugs, including mitomycin C, cisplatin, and 5-fluorouracil, *in vitro* and *in vivo* (26–28). UCN-01 is currently in the phase II study of its effects on relapsed or refractory systemic anaplastic large cell and mature T-cell lymphomas (29, 30). UCN-01 was initially administered as a 72-h continuous infusion every 2 weeks, based on data from *in vitro* and xenograft preclinical models. However, in the first few patients, the drug had an unexpectedly long half-life (>30 days), which was 100 times longer than the

* The costs of publication of this article were defrayed in part by the payment of page charges. This article must therefore be hereby marked "*advertisement*" in accordance with 18 U.S.C. Section 1734 solely to indicate this fact.

** To whom correspondence should be addressed: Dept. of Biopharmaceutics, Graduate School of Pharmaceutical Sciences, Kumamoto University, 5-1 Oe-honmachi, Kumamoto, 862-0973, Japan. Tel.: 81-96-3714150; Fax: 81-96-3627690; E-mail: otagirim@gpo.kumamoto-u.ac.jp.

[1] The abbreviations used are: hAGP, human α1-acid glycoprotein; UCN-01, 7-hydroxystaurosporine; rhAGP, recombinant hAGP; PVDF, polyvinylidene difluoride; HPLC, high performance liquid chromatography; PKC, protein kinase C.

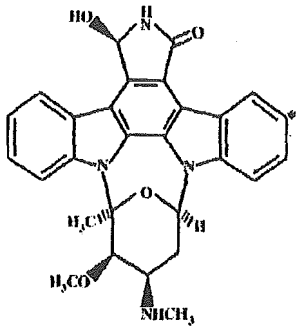

FIG. 1. **Chemical structure of [^{3}H]UCN-01.** *, ^{3}H-labeled position.

half-life observed in preclinical models. The distribution volumes (0.0796~0.158 liter/kg) and systemic clearance (0.0407~0.252 ml/h/kg) in the human patients were found to be extremely low. This pharmacokinetic behavior of UCN-01 in humans can partly be attributed to its specific high affinity binding to hAGP, which causes slow dissociation of UCN-01 from hAGP and thereby limits its disposition and elimination (31, 32). The binding constant for UCN-01 and hAGP, 8×10^8 M^{-1}, is the highest value ever reported for protein binding studies (33).

Several protein binding studies of hAGP had been conducted using a variety of techniques including equilibrium dialysis, ultrafiltration, chemical modification, and displacement (34–37). In a recent study, we identified the key factors contributing to the unusually high binding affinity between UCN-01 and hAGP: the substituent at C-7 of the UCN-01 molecule, and the Trp residues of hAGP (38). Crystallographic structural analysis has become more common and appears to be a good method for analysis of ligand-protein interaction, but there have been no reports of crystallographic structural analysis of hAGP. Certain experimental techniques allow direct evaluation of ligand-protein complexes, which can elucidate the binding chemistry of hAGP. Photoaffinity labeling is an essential complement to modeling and mutagenesis and allows direct, unambiguous identification of the contact region between a binding protein and its specific photoactivatable ligands (39–41). There is no photoaffinity labeling study that has led to the direct determination of labeled amino acid residues in hAGP. In the present study, we used [^{3}H]UCN-01 (Fig. 1) as a photoaffinity labeling agent to characterize the binding site of hAGP. Also, single residue mutants of recombinant hAGP (W25A, W122A, and W160A) were produced in order to determine which Trp was involved in the high affinity binding of [^{3}H]UCN-01. Finally, we constructed models of the docking of UCN-01 into the binding cavity, using a three-dimensional molecular model of hAGP.

EXPERIMENTAL PROCEDURES

Materials—[^{3}H]UCN-01 (12 Ci/mmol), UCN-01, UCN-02, and staurosporine were supplied by Kyowa Hakko Kogyo Co. (Shizuoka, Japan). hAGP (purified from cohn fraction VI) was purchased from Sigma. Sequencing grade modified trypsin was purchased from Promega. All other chemicals and solvents were of analytical grade. *N*-Glycosidase F recombinant (PNGase F) was purchased from Roche Applied Science. Plasma-derived AGP (pAGP), propranolol, and progesterone were purchased from Sigma. Potassium warfarin was donated by Eisai Co. (Tokyo, Japan). Restriction enzymes, *Escherichia coli* JM109, the DNA ligation kit, and the DNA polymerase Premix Taq® (EX Taq version) were obtained from Takara Biotechnology Co. Ltd. (Kyoto, Japan). The DNA sequencing kit was obtained from PerkinElmer Applied Biosystems (Tokyo, Japan). The Pichia expression kit was purchased from Invitrogen. DEAE Sephacel, phenyl-Sepharose Fast Flow, and Sephadex G-75 superfine were purchased from Amersham Biosciences.

Expression and Purification of Wild-type and Mutant rhAGP—Recombinant hAGP (rhAGP) was expressed in the methylotropic yeast *Pichia pastoris* using the expression vector pPIC9, and was purified by anionic exchange, hydrophobic interaction, and gel filtration chromatography (42). The single residue mutants W25A, W122A, and W160A were prepared using a QuikChange® XL site-directed mutagenesis kit, following the procedure of Braman *et al.* (43).

Purification of rhAGP—The growth medium was separated from the yeast by centrifugation (6000 × *g*, 10 min, 4 °C), and the secreted rhAGP was isolated from the medium as follows. The medium was brought to 60% saturation with ammonium sulfate at room temperature. The temperature was then lowered to 4 °C, and the pH was adjusted to 4.0. After shaking for 12 h, the precipitated protein was collected by centrifugation (12,000 × *g*, 60 min, 4 °C) and resuspended in distilled water. Dialysis was performed for 48 h at 4 °C against 100 volumes of distilled water, followed by a further 24 h of dialysis against 100 volumes of 10 mM Tris-HCl buffer (pH 7.4). Then, the solution was loaded onto a column of DEAE Sephacel. rhAGP was eluted with a linear gradient of 0–1 M NaCl in 10 mM Tris-HCl buffer (pH 7.4). The eluted rhAGP was loaded onto a column of phenyl-Sepharose Fast Flow. Finally, rhAGP was purified using Sephadex G-75 superfine resin.

Photoaffinity Labeling of hAGP—hAGP (50 μM) was incubated with [^{3}H]UCN-01 (0.08 μM) in 100 μl of 20 mM Tris-HCl (pH 7.4) in a 1.5-ml Eppendorf tube at room temperature in the dark for 60 min. The incubation mixture was then placed on ice and irradiated for 30 min by a 100-watt black light/blue lamp (310 nm, Ultra-Violet Products, Inc., San Gabriel, CA) at a distance of 10 cm. After irradiation, the photolabeled hAGP was precipitated by adding 1 ml of acetone, followed by centrifugation at 15 × 1000 rpm for 10 min. The pellet was washed with 1 ml of ethanol and centrifuged a second time.

SDS-PAGE and Electroblotting—Photolabeled hAGP was analyzed by SDS-PAGE using a 10% polyacrylamide gel (according to the method of Laemmli) and a sampling buffer (10 mM Tris-HCl, pH 7.6, 1% (w/v) SDS, 20 mM dithiothreitol, 4 mM EDTA, and 2% (w/v) sucrose). The concentration of protein was determined by Bradford assay using bovine serum albumin as the standard (44). After electrophoresis, the gel was electrophoretically transferred onto a PVDF membrane in a transfer buffer (25 mM Tris, 193 mM glycine, 10% methanol) using a semidry blotting assembly. The blotted membrane was stained with Coomassie Brilliant Blue R250, followed by complete drying in air.

Autoradiograpic Analysis—For autoradiographic analysis, the dried PVDF membrane was placed in contact with an imaging plate (BAS III, Fuji Photo Film Co.) in a cassette (BAS cassette 2040) at room temperature for 48 h. The imaging plate was scanned and analyzed using a Bio-Imaging Analyzer (model BAS FLA-3000 G; Fuji Photo Film Co.), and was then analyzed using L Process V1.6 software (Fuji Film Science Lab 98). The incorporation of radioactivity into individual fragments was quantified using Image Gauge V3.1 software (Fuji Film).

Competition Experiments—In order to determine the photolabeling specificity of the binding site of [^{3}H]UCN-01, hAGP (50 μM) was incubated with [^{3}H]UCN-01 (0.08 μM) in the presence of competitors (250 μM) prior to photolysis. The competitors were the UCN-01 analogues staurosporine and UCN-02, the basic drug propranolol, the acidic drug warfarin, and progesterone (representative steroid hormone). The photolabeled hAGP was separated by 10% gel SDS-PAGE and electroblotted onto a PVDF membrane before being subjected to autoradiographic analysis.

Reductive Pyridylethylation and Deglycosylation of hAGP—After the photolabeled hAGP was precipitated by acetone, 100 μl of the buffer was added to the precipitate. Then, 10 μl of 1% SDS and 1 M 2-mercaptoethanol were added to this solution, followed by reduction at 100 °C at 10 min. For deglycosylation of hAGP, 10 μl of 10% *n*-octanoyl-*N*-methylglucamide (MEGA-8), 50 μl of deionized water and 2 units of PNGase F were added to the reduction solution, and the resulting solution was incubated for 24 h. Then, 1 μl of 4-vinylpyridine was added, the mixture was further incubated in a N_2 atmosphere for 30 min at room temperature in the dark, and was then dialyzed for desalination.

Tryptic Digestion and Purification of Photolabeled hAGP Peptide Fragments—Tryptic digestion was performed in 50 mM NH_4HCO_3 (pH 7.8). After deglycosylation, deglycosylated hAGP was incubated with trypsin for 5 h at 37 °C. The ratio of trypsin to hAGP was 1:20 (w/w). Tryptic peptides were separated by reverse-phase C_{18} column (5 μm, 4.6 × 250 mm, Vydac) high performance liquid chromatography (HPLC) using an aqueous acetonitrile gradient in the presence of 0.1% trifluoroacetic acid. The separated peptides were fractionated every 30 s; 200 μl of each fraction were added to 2.5 ml of scintillation mixture; and the radioactivity was determined using a LSC-500 liquid scintillation counter (Aloka, Tokyo, Japan). The fraction with the highest radioactivity was collected in an Eppendorf tube, and was evaporated on a SpeedVac